Journal of Sound and Vibration (2003) **259**(3), 649–675
doi:10.1006/jsvi.2002.5098, available online at http://www.idealibrary.com on IDEAL®

DYNAMICS OF A TWO-CRACK ROTOR

A. K. Darpe, K. Gupta and A. Chawla

Department of Mechanical Engineering, Indian Institute of Technology, Hauz Khas, New Delhi 110016*, India. E-mail: kgupta@mech.iitd.ernet.in*

(*Received* 29 *October* 2001, *and in final form* 15 *February* 2002)

The effect of the presence of the single transverse crack on the response of the rotor has been a focus of attention for many researchers. In the present work a simple Jeffcott rotor with two transverse surface cracks has been studied. The stiffness of such a rotor is derived based on the concepts of fracture mechanics. Subsequently, the effect of the interaction of the two cracks on the breathing behavior and on the unbalance response of the rotor is studied. When the angular orientation of one crack relative to the other is varied, significant changes in the dynamic response of the rotor are noticed. A special case of practical importance of a two-crack rotor is one when one of the cracks is assumed to remain open always whereas the other can breathe like a fatigue crack. This simulates a transverse crack in an asymmetric rotor. Effect of orientation of the breathing crack with respect to the open crack on the dynamic response is studied in detail. The results of the present study will be useful in diagnosing fatigue cracks in real rotors, which invariably have some asymmetry.

1. INTRODUCTION

Fatigue cracks because of their potential to cause catastrophic failures are a grave threat to an uninterrupted operation and performance of the modern day machines. Since mid-1970 various researchers have studied the response of a cracked rotor. The work on the diagnosis of crack has been mainly based on vibration signature. The changes in the vibration response in the form of changes of frequency composition or a rising trend of higher harmonics of rotational frequency or an increased level of subharmonic resonances have been found to be some of the important crack indicators. These vibration-based techniques have been applied to a variety of engineering structures, such as beams, trusses, rotors, etc. The research in the past few decades on cracked structures and rotors is well documented in review papers by Wauer [1] and Dimarogonas [2].

The thrust of most of the works in the past has been on a structure with a single transverse surface crack. When more than one crack appears in a structure, the dynamic response becomes more complex depending upon the relative positions and depths of these cracks. Moreover various combinations of position and depth can lead to the identical changes in the natural frequencies. Various investigators have recently addressed the effect of two surface cracks on the vibration response of structures. Ostachowicz and Krawczuk [3] analyzed the effect of positions and depths of two cracks on the natural frequency of cantilever beams. Shen and Pierre [4] considered a pair of symmetric cracks at mid-span and focussed their attention on the effect of these cracks on the mode shapes. Both the Galerkin procedure and the finite element approach have been used. Effect of crack depth and location on the eigenfrequencies of a double cracked beam has also been studied [5].

0022-460X/02/$35.00

A review based on the work related to multiple cracked structures is presented by Ruotolo and Surace [6]. Development of generalized damage identification procedures for systems with multiple cracks based on optimization [7] and genetic algorithm [8] has received considerable attention recently.

The problem of two cracks in a rotor has not been dealt with in detail until now. Recently, Sekhar [9] carried out a parametric study of two transverse open cracks in a rotor and studied the effect of various crack parameters on the eigenfrequencies and stability speeds of rotors. He used finite element model of a rotor bearing system for flexural vibrations and carried out a study on two aligned open cracks.

In the present study the dynamic response analysis of two-crack rotor is carried out. A simple Jeffcott rotor with two transverse surface cracks is considered. A more realistic breathing crack model is used as against the open crack model applied in earlier studies. The cracks are assumed at some distance apart near the mid-span. The stiffness of the Jeffcott rotor due to the presence of these cracks is derived based on fracture mechanics concepts. Then the dynamic response of the cracked Jeffcott rotor is obtained for an unbalance excitation. The effects of orientation of one crack relative to the other on the unbalance response and on the breathing behaviour of the two cracks are studied. A special case of the two-crack rotor is when one of the cracks is of open type while the other can breathe during the rotation of rotor. This simulates an asymmetric rotor with a fatigue crack. This case is studied in detail to estimate the effect of the presence of fatigue crack on the response of an asymmetric rotor. Such a study of an asymmetric shaft having a transverse crack has not been attempted. The only related work is by Lees and Friswell [10]. They discussed the effect of chordal cracks on the mode shapes of asymmetric rotors and also studied the effect of orientation of the rotor on various modes of vibration.

In the following section the stiffness of a two-crack Jeffcott rotor is derived. Then in section 3, unbalance response of the two-crack rotor is studied for various speeds and orientation angle between two cracks. Section 4 discusses the response of an asymmetric rotor with a breathing transverse crack. The important findings of the present work are summarized in section 5.

2. STRIFFNESS OF A TWO-CRACK ROTOR

Consider a Jeffcott rotor that has two transverse surface cracks with one oriented from the other at an angle of γ as shown in Figure 1. The cracks assumed to be some distance apart axially so as not to influence the stress fields of one another, but assumed close enough to be located at midspan.

Here an attempt is made to find the flexibility of a cracked Jeffcott rotor with two transverse surface cracks oriented in rotor-fixed directions ξ_1 and ξ_2 are shown in Figure 1. Co-ordinate system for crack 1 is $\xi_1-\eta_1$ and that for crack 2 is $\xi_2-\eta_2$, the orientation angle between them being γ. Q_{ξ_1} and Q_{η_1} are the forces on the rotor in $\xi_1-\eta_1$ co-ordinates at the center of the span of the rotor where the two cracks are situated. In $\xi_2-\eta_2$ co-ordinates these forces are denoted by Q_{ξ_2} and Q_{η_2}. They are related as follows:

$$\begin{Bmatrix} Q_{\xi_2} \\ Q_{\eta_2} \end{Bmatrix} = \begin{bmatrix} \cos\gamma & \sin\gamma \\ -\sin\gamma & \cos\gamma \end{bmatrix} \begin{Bmatrix} Q_{\xi_1} \\ Q_{\eta_1} \end{Bmatrix}. \tag{1}$$

The cracks open and close during a rotation, i.e., they breathe under the influence of gravity and unbalance forces acting on the crack cross-section. The flexibility of the cracked rotor is a function of the amount of crack opening of both these cracks. Thus the flexibility of the two-crack rotor is constantly changing. The amount of crack opening for

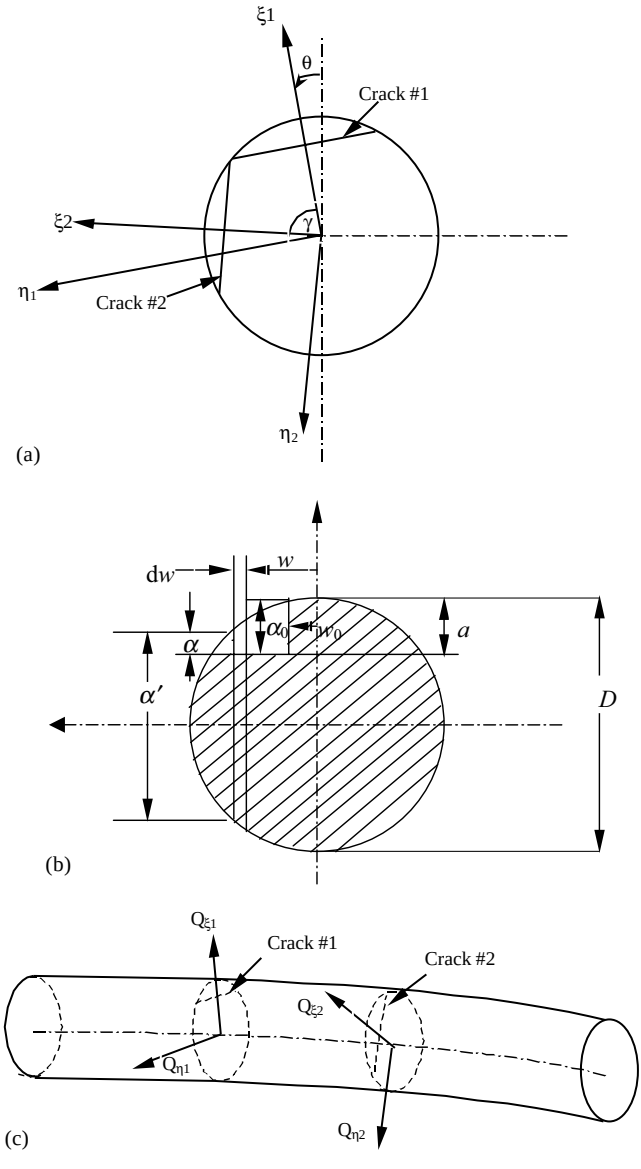

Figure 1. Details of a two-crack Jeffcott rotor. (a) Co-ordinate system. (b) Details of a crack cross-section. (c) Forces acting on the rotor at the crack cross-sections.

each crack depends on the stresses acting on the crack edge. The stress intensity factor (K_1^I) on the crack is given below [11, 12]:

$$K_1^I = K_{Q_{\xi_1}}^I + K_{Q_{\eta_1}}^I. \tag{2}$$

Here

$$K_{Q_{\xi_1}}^I = \sigma_{\xi_1}\sqrt{\pi\alpha}F, \quad \sigma_{\xi_1} = \frac{\left(\dfrac{Q_{\xi_1}L}{4}\right)\dfrac{\alpha'}{2}}{I}, \quad K_{Q_{\xi_1}}^I = \frac{Q_{\xi_1}L\alpha'}{8I}\sqrt{\pi\alpha}F \tag{3}$$

and

$$K^I_{Q_{\eta_1}} = \sigma_{\eta_1}\sqrt{\pi\alpha}F', \quad \sigma_{\eta_1} = \frac{\left(\frac{Q_{\eta_1}L}{4}\right)w}{I}, \quad K^I_{Q_{\eta_1}} = \frac{Q_{\eta_1}Lw}{4I}\sqrt{\pi\alpha}F', \tag{4}$$

where $I = (\pi/64)d^4$ and functions F and F', which depend on crack parameters α and α', are given as under

$$F = \sqrt{\frac{2\alpha'}{\pi\alpha}\tan\left(\frac{\pi\alpha}{2\alpha'}\right)}\,\frac{0{\cdot}923 + 0{\cdot}199\left[1 - \sin\left(\frac{\pi\alpha}{2\alpha'}\right)\right]^4}{\cos\left(\frac{\pi\alpha}{2\alpha'}\right)},$$

$$F' = \sqrt{\frac{2\alpha'}{\pi\alpha'}\tan\left(\frac{\pi\alpha}{2\alpha'}\right)}\,\frac{0{\cdot}752 + 2{\cdot}02\left(\frac{\alpha}{\alpha'}\right) + 0{\cdot}37\left[1 - \sin\left(\frac{\pi\alpha}{2\alpha'}\right)\right]^3}{\cos\left(\frac{\pi\alpha}{2\alpha'}\right)}. \tag{5}$$

From fracture mechanics, the additional deflection due to the presence of crack in $\xi_1-\eta_1$ co-ordinates is

$$u_{i_1} = \frac{\partial}{\partial Q_{i_1}}\left[\int J_1(\alpha)\,\mathrm{d}\alpha\right], \tag{6}$$

where strain energy density function is given as

$$J_1(\alpha) = \frac{1}{E}[K^I_{Q_{\xi_1}} + K^I_{Q_{\eta_1}}]^2. \tag{7}$$

Substituting equation (7) in equation (6) and using relation (3) and (4), we get

$$u_{\xi_1} = \frac{2}{E}\int\int_{A_1}\left(\frac{Q_{\xi_1}L\alpha'\sqrt{\pi\alpha}F}{8I} + \frac{Q_{\eta_1}Lw}{4I}\sqrt{\pi\alpha}F'\right)\frac{L\alpha'\sqrt{\pi\alpha}F}{8I}\,\mathrm{d}\alpha\,\mathrm{d}w, \tag{8}$$

$$u_{\eta_1} = \frac{2}{E}\int\int_{A_1}\left(\frac{Q_{\xi_1}L\alpha'\sqrt{\pi\alpha}F}{8I} + \frac{Q_{\eta_1}Lw}{4I}\sqrt{\pi\alpha}F'\right)\frac{Lw\sqrt{\pi\alpha}F'}{4I}\,\mathrm{d}\alpha\,\mathrm{d}w. \tag{9}$$

Similarly additional deflection in $\xi_2-\eta_2$ co-ordinate for crack 2 can be shown to be

$$u_{\xi_2} = \frac{2}{E}\int\int_{A_2}\left(\frac{Q_{\xi_2}L\alpha'\sqrt{\pi\alpha}F}{8I} + \frac{Q_{\eta_2}Lw}{4I}\sqrt{\pi\alpha}F'\right)\frac{L\alpha'\sqrt{\pi\alpha}F}{8I}\,\mathrm{d}\alpha\,\mathrm{d}w, \tag{10}$$

$$u_{\eta_2} = \frac{2}{E}\int\int_{A_2}\left(\frac{Q_{\xi_2}L\alpha'\sqrt{\pi\alpha}F}{8I} + \frac{Q_{\eta_2}Lw}{4I}\sqrt{\pi\alpha}F'\right)\frac{Lw\sqrt{\pi\alpha}F'}{4I}\,\mathrm{d}\alpha\,\mathrm{d}w. \tag{11}$$

In equations (8)–(11), the areas of integration A_1 and A_2 denote the open part of the cracks 1 and 2 respectively.

Using equation (1), the above displacements in terms of forces acting on crack 1 are

$$\begin{aligned} u_{\xi_2} =& \frac{2}{E}\int\int_{A_2}\left[\left(\frac{(Q_{\xi_1}\cos\gamma + Q_{\eta_1}\sin\gamma)L\alpha'\sqrt{\pi\alpha}F}{8I}\right.\right. \\ &\left.\left. + \frac{(-Q_{\xi_1}\sin\gamma + Q_{\eta_1}\cos\gamma)Lw\sqrt{\pi\alpha}F'}{4I}\right)\right]\frac{L\alpha'\sqrt{\pi\alpha}F}{8I}\,\mathrm{d}\alpha\,\mathrm{d}w \\ =& \frac{2}{E}\int\int_{A_2}\left[\left[\frac{L^2\alpha'^2\pi\alpha F^2}{64I^2}\cos\gamma - \frac{L^2\alpha' w\pi\alpha FF'}{32I^2}\sin\gamma\right]Q_{\xi_1}\right. \\ &\left. + \left[\frac{L^2\alpha'^2\pi\alpha F^2}{64I^2}\sin\gamma + \frac{L^2 w\alpha'\pi\alpha FF'}{32I^2}\cos\gamma\right]Q_{\eta_1}\right]\mathrm{d}\alpha\,\mathrm{d}w, \end{aligned} \tag{12}$$

$$u_{\eta_2} = \frac{2}{E}\int\int_{A_2}\left[\left(\frac{(Q_{\xi_1}\cos\gamma + Q_{\eta_1}\sin\gamma)L\alpha'\sqrt{\pi\alpha}F}{8I}\right.\right.$$

$$\left.\left. + \frac{(Q_{\eta_1}\cos\gamma - Q_{\xi_1}\sin\gamma)Lw\sqrt{\pi\alpha}F'}{4I}\right)\right]\frac{Lw\sqrt{\pi\alpha}F'}{4I}\,\mathrm{d}\alpha\,\mathrm{d}w$$

$$= \frac{2}{E}\int\int_{A_2}\left[\left[\frac{L^2\alpha' w\pi\alpha FF'}{32I^2}\cos\gamma - \frac{L^2w^2\pi\alpha F'^2}{16I^2}\sin\gamma\right]Q_{\xi_1}\right.$$

$$\left. + \left[\frac{L^2\alpha'^2\pi\alpha FF'}{32I^2}\sin\gamma + \frac{L^2w^2\pi\alpha F'^2}{16I^2}\cos\gamma\right]Q_{\eta_1}\right]\mathrm{d}\alpha\,\mathrm{d}w. \tag{13}$$

Deflections in direction ξ_1 is written as

$$\hat{u}_{\xi_1} = u_{\xi_1} + u_{\xi_2}\cos\gamma - u_{\eta_2}\sin\gamma + u^0_{\xi_1}. \tag{14}$$

Here, u_{ξ_1} is the deflection due to crack 1 in the direction ξ_1, u_{ξ_2} the deflection due to crack 2 in the direction ξ_2, u_{η_2} the deflection due to crack 2 in the direction η_2, and $u^0_{\xi_1}$ the deflection of uncracked shaft in the ξ_1 direction:

$$u^0_{\xi_1} = \frac{Q_{\xi_1}L^3}{48EI}. \tag{15}$$

Using equations (8), (12), (13) and (15), equation (14) can be written as

$$\hat{u}_{\xi_1} = \frac{2}{E}\int\int_{A_1}\left(\frac{Q_{\xi_1}L\alpha'\sqrt{\pi\alpha}F}{8I} + \frac{Q_{\eta_1}Lw}{4I}\sqrt{\pi\alpha}F'\right)\frac{L\alpha'\sqrt{\pi\alpha}F}{8I}\,\mathrm{d}\alpha\,\mathrm{d}w$$

$$+ \frac{2}{E}\int\int_{A_2}\left[\begin{array}{l}\left[\dfrac{L^2\alpha'^2\pi\alpha F^2}{64I^2}\cos\gamma - \dfrac{L^2\alpha' w\pi\alpha FF'}{32I^2}\sin\gamma\right]Q_{\xi_1} + \\ \left[\dfrac{L^2\alpha'^2\pi\alpha F^2}{64I^2}\sin\gamma + \dfrac{L^2\alpha' w\pi\alpha FF'}{32I^2}\cos\gamma\right]Q_{\eta_1}\end{array}\right]\cos\gamma\,\mathrm{d}\alpha\,\mathrm{d}w$$

$$- \frac{2}{E}\int\int_{A_2}\left[\begin{array}{l}\left[\dfrac{L^2\alpha' w\pi\alpha FF'}{32I^2}\cos\gamma - \dfrac{L^2w^2\pi\alpha F'^2}{16I^2}\sin\gamma\right]Q_{\xi_1} + \\ \left[\dfrac{L^2\alpha' w\pi\alpha FF'}{32I^2}\sin\gamma + \dfrac{L^2w^2\pi\alpha F'^2}{16I^2}\cos\gamma\right]Q_{\eta_1}\end{array}\right]\sin\gamma\,\mathrm{d}\alpha\,\mathrm{d}w + \frac{Q\xi_1L^3}{48EI}. \tag{16}$$

Similarly for direction η_1

$$\hat{u}_{\eta_1} = u_{\eta_1} + u_{\xi_2}\sin\gamma + u_{\eta_2}\cos\gamma + u^0_{\eta_1}. \tag{17}$$

Here, u_{η_1} is the deflection due to crack 1 in direction η_1, u_{ξ_2} the deflection due to crack 2 in direction ξ_2, u_{η_2} the deflection due to crack 2 in direction η_2, and $u^0_{\eta_1}$ the deflection of uncracked shaft in η_1 direction:

$$u^0_{\eta_1} = \frac{Q_{\eta_1}L^3}{48EI}. \tag{18}$$

Using equations (9), (12), (13) and (18), equation (17) can be written as

$$\hat{u}_{\eta_1} = \frac{2}{E}\int\int_{A_1}\left(\frac{Q_{\xi_1}L\alpha'\sqrt{\pi\alpha}F}{8I} + \frac{Q_{\eta_1}Lw}{4I}\sqrt{\pi\alpha}F'\right)\frac{Lw\sqrt{\pi\alpha}F'}{4I}\,\mathrm{d}\alpha\,\mathrm{d}w$$
$$+\frac{2}{E}\int\int_{A_2}\begin{bmatrix}\left[\frac{L^2\alpha'^2\pi\alpha F^2}{64I^2}\cos\gamma - \frac{L^2\alpha' w\pi\alpha FF'}{32I^2}\sin\gamma\right]Q_{\xi_1} + \\ \left[\frac{L^2\alpha'^2\pi\alpha F^2}{64I^2}\sin\gamma + \frac{L^2\alpha' w\pi\alpha FF'}{32I^2}\cos\gamma\right]Q_{\eta_1}\end{bmatrix}\sin\gamma\,\mathrm{d}\alpha\,\mathrm{d}w$$
$$+\frac{2}{E}\int\int_{A_2}\begin{bmatrix}\left[\frac{L^2\alpha' w\pi\alpha FF'}{32I^2}\cos\gamma - \frac{L^2w^2\pi\alpha F'^2}{16I^2}\sin\gamma\right]Q_{\xi_1} + \\ \left[\frac{L^2\alpha' w\pi\alpha FF'}{32I^2}\sin\gamma + \frac{L^2w^2\pi\alpha F'^2}{16I^2}\cos\gamma\right]Q_{\eta_1}\end{bmatrix}\cos\gamma\,\mathrm{d}\alpha\,\mathrm{d}w + \frac{Q\eta_1L^3}{48EI}. \quad (19)$$

The direct and cross-coupled flexibility values g_ξ, g_η, $g_{\xi\eta}$, $g_{\eta\xi}$ can now be found as follows:

$$g_\xi = \frac{\partial\hat{u}_{\xi_1}}{\partial Q_{\xi_1}}.$$

From equation (16), we have

$$g_\xi = \frac{2}{E}\int_{A_1}\left(\frac{L^2\alpha'^2\pi\alpha F^2}{64I^2}\,\mathrm{d}\alpha\,\mathrm{d}w\right)$$
$$+\frac{2}{E}\int\int_{A_2}\left[\frac{L^2\alpha'^2\pi\alpha F^2}{64I^2}\cos^2\gamma - \frac{L^2\alpha' w\pi\alpha FF'}{32I^2}\sin\gamma\cos\gamma\right]\mathrm{d}\alpha\,\mathrm{d}w$$
$$-\frac{2}{E}\int\int_{A_2}\left[\frac{L^2\alpha' w\pi\alpha FF'}{32I^2}\sin\gamma\cos\gamma - \frac{L^2w^2\pi\alpha F'^2}{16I^2}\sin^2\gamma\right]\mathrm{d}\alpha\,\mathrm{d}w + \frac{L^3}{48EI} \quad (20)$$

and

$$g_{\xi\eta} = \frac{\partial\hat{u}_{\xi_1}}{\partial Q_{\eta_1}},$$

$$g_{\xi\eta} = \frac{2}{E}\int_{A_1}\left(\frac{L^2w\alpha'\pi\alpha FF'}{32I^2}\,\mathrm{d}\alpha\,\mathrm{d}w\right)$$
$$+\frac{2}{E}\int\int_{A_2}\left[\frac{L^2\alpha'^2\pi\alpha F^2}{64I^2}\sin\gamma\cos\gamma + \frac{L^2\alpha' w\pi\alpha FF'}{32I^2}\cos^2\gamma\right]\mathrm{d}\alpha\,\mathrm{d}w$$
$$-\frac{2}{E}\int\int_{A_2}\left[\frac{L^2\alpha' w\pi\alpha FF'}{32I^2}\sin^2\gamma + \frac{L^2w^2\pi\alpha F'^2}{16I^2}\sin\gamma\cos\gamma\right]\mathrm{d}\alpha\,\mathrm{d}w, \quad (21)$$

$$g_\eta = \frac{\partial\hat{u}_{\eta_1}}{\partial Q_{\eta_1}},$$

so from equation (19), we have

$$g_\eta = \frac{2}{E}\int_{A_1}\left(\frac{L^2w^2\pi\alpha F'^2}{16I^2}\,\mathrm{d}\alpha\,\mathrm{d}w\right)$$
$$+\frac{2}{E}\int\int_{A_2}\left[\frac{L^2\alpha'^2\pi\alpha F^2}{64I^2}\sin^2\gamma + \frac{L^2\alpha' w\pi\alpha FF'}{32I^2}\sin\gamma\cos\gamma\right]\mathrm{d}\alpha\,\mathrm{d}w$$
$$-\frac{2}{E}\int\int_{A_2}\left[\frac{L^2\alpha' w\pi\alpha FF'}{32I^2}\sin\gamma\cos\gamma + \frac{L^2w^2\pi\alpha F'^2}{16I^2}\cos^2\gamma\right]\mathrm{d}\alpha\,\mathrm{d}w + \frac{L^3}{48EI}. \quad (22)$$

Also,

$$g_{\eta\xi} = \frac{\partial \hat{u}_{\eta_1}}{\partial Q_{\xi_1}},$$

and it can be shown that

$$g_{\xi\eta} = g_{\eta\xi}. \tag{23}$$

The equations for flexibility (equations (20)–(23)) are rewritten as follows:

$$\begin{aligned} g_\xi = {} & \frac{\pi L^2}{32EI^2}\int\int_{A_1} \alpha'^2 \alpha F^2 \,\mathrm{d}\alpha\,\mathrm{d}w + \frac{\pi L^2 \cos^2\gamma}{32EI^2}\int\int_{A_2} \alpha'^2 \alpha F^2 \,\mathrm{d}\alpha\,\mathrm{d}w \\ & - \frac{\pi L^2 \sin\gamma\cos\gamma}{16EI^2}\int\int_{A_2} \alpha'^2 w\alpha FF' \,\mathrm{d}\alpha\,\mathrm{d}w - \frac{\pi L^2 \sin\gamma\cos\gamma}{16EI^2}\int\int_{A_2} \alpha' w\alpha FF' \,\mathrm{d}\alpha\,\mathrm{d}w \\ & + \frac{\pi L^2 \sin^2\gamma}{8EI^2}\int\int_{A_2} w^2 \alpha F'^2 \,\mathrm{d}\alpha\,\mathrm{d}w + \frac{L^3}{48EI} \end{aligned} \tag{24}$$

and

$$\begin{aligned} g_\eta = {} & \frac{\pi L^2}{8EI^2}\int\int_{A_1} w^2 \alpha F'^2 \,\mathrm{d}\alpha\,\mathrm{d}w + \frac{\pi L^2 \sin^2\gamma}{32EI^2}\int\int_{A_2} \alpha'^2 \alpha F^2 \,\mathrm{d}\alpha\,\mathrm{d}w \\ & + \frac{\pi L^2 \sin\gamma\cos\gamma}{16EI^2}\int\int_{A_2} w\alpha' \alpha FF' \,\mathrm{d}\alpha\,\mathrm{d}w + \frac{\pi L^2 \sin\gamma\cos\gamma}{16EI^2}\int\int_{A_2} w\alpha' \alpha FF' \,\mathrm{d}\alpha\,\mathrm{d}w \\ & + \frac{\pi L^2 \cos^2\gamma}{8EI^2}\int\int_{A_2} w^2 \alpha F'^2 \,\mathrm{d}\alpha\,\mathrm{d}w + \frac{L^3}{48EI}, \end{aligned} \tag{25}$$

$$\begin{aligned} g_{\xi\eta} = g_{\eta\xi} = {} & \frac{\pi L^2}{16EI^2}\int\int_{A_1} w\alpha' \alpha FF' \,\mathrm{d}\alpha\,\mathrm{d}w + \frac{\pi L^2 \sin\gamma\cos\gamma}{32EI^2}\int\int_{A_2} \alpha'^2 \alpha F^2 \,\mathrm{d}\alpha\,\mathrm{d}w \\ & + \frac{\pi L^2 \cos^2\gamma}{16EI^2}\int\int_{A_2} w\alpha' \alpha FF' \,\mathrm{d}\alpha\,\mathrm{d}w - \frac{\pi L^2 \sin^2\gamma}{16EI^2}\int\int_{A_2} w\alpha' \alpha FF' \,\mathrm{d}\alpha\,\mathrm{d}w \\ & - \frac{\pi L^2 \sin\gamma\cos\gamma}{8EI^2}\int\int_{A_2} w^2 \alpha F'^2 \,\mathrm{d}\alpha\,\mathrm{d}w. \end{aligned} \tag{26}$$

These can be further written as

$$g_\xi = \frac{\pi L^2}{32EI^2} I'_{g1} + \frac{\pi L^2 \cos^2\gamma}{32EI^2} I''_{g1} - \frac{\pi L^2 \sin\gamma\cos\gamma}{8EI^2} I''_{g2} + \frac{\pi L^2 \sin^2\gamma}{8EI^2} I''_{g3} + \frac{L^3}{48EI}, \tag{27}$$

$$g_\eta = \frac{\pi L^2}{32EI^2} I'_{g2} + \frac{\pi L^2 \sin^2\gamma}{32EI^2} I''_{g1} + \frac{\pi L^2 \sin\gamma\cos\gamma}{8EI^2} I''_{g2} - \frac{\pi L^2 \cos^2\gamma}{8EI^2} I''_{g3} + \frac{L^3}{48EI}, \tag{28}$$

$$g_{\xi\eta} = \frac{\pi L^2}{16EI^2} I'_{g3} + \frac{\pi L^2 \sin\gamma\cos\gamma}{32EI^2} I''_{g1} - \frac{\pi L^2(\cos^2\gamma - \sin^2\gamma)}{16EI^2} I''_{g2} + \frac{\pi L^2 \sin\gamma\cos\gamma}{8EI^2} I''_{g3}, \tag{29}$$

where

$$I'_{g1} = \int\int_{A_1} \alpha'^2 \alpha F^2 \,\mathrm{d}\alpha\,\mathrm{d}w, \quad I'_{g2} = \int\int_{A_1} w^2 \alpha F'^2 \,\mathrm{d}\alpha\,\mathrm{d}w, \quad I'_{g3} = \int\int_{A_1} w\alpha' \alpha FF' \,\mathrm{d}\alpha\,\mathrm{d}w,$$

$$I''_{g1} = \int\int_{A_2} \alpha'^2 \alpha F^2 \,\mathrm{d}\alpha\,\mathrm{d}w, \quad I''_{g2} = \int\int_{A_2} w\alpha' \alpha FF' \,\mathrm{d}\alpha\,\mathrm{d}w, \quad I''_{g3} = \int\int_{A_2} w^2 \alpha F'^2 \,\mathrm{d}\alpha\,\mathrm{d}w. \tag{30}$$

It may be noted that for $\gamma = 0^\circ$, the above expressions reduce to flexibility expressions similar to those given by June *et al.* [11]. The stiffness coefficients can now be

obtained as

$$k_\eta = \frac{g_\xi}{g_\xi g_\eta - g_{\xi\eta}^2}, \quad k_{\xi\eta} = k_{\eta\xi} = \frac{-g_{\xi\eta}}{g_\xi g_\eta - g_{\xi\eta}^2}, \quad k_\xi = \frac{g_\eta}{g_\xi g_\eta - g_{\xi\eta}^2}. \tag{31}$$

Using these stiffness coefficients the equation of motion can be written as [13]

$$m(\ddot{\xi}_1 - 2\omega\dot{\eta}_1 - \omega^2\xi_1) + c(\dot{\xi}_1 - \omega\eta_1) + k_\xi\xi_1 + k_{\xi\eta}\eta_1 = m\varepsilon\omega^2\cos\beta - mg\cos\theta,$$

$$m(\ddot{\eta}_1 - 2\omega\dot{\xi}_1 - \omega^2\eta_1) + c(\dot{\eta}_1 - \omega\xi_1) + k_{\eta\xi}\xi_1 + k_\eta\eta_1 = m\varepsilon\omega^2\sin\beta - mg\sin\theta. \tag{32}$$

The response obtained using these equations can be used to estimate the forces on the crack cross-section as follows:

$$\begin{Bmatrix} Q_{\xi_1} \\ Q_{\eta_1} \end{Bmatrix} = \begin{bmatrix} k_\xi & k_{\xi\eta} \\ k_{\eta\xi} & k_\eta \end{bmatrix} \begin{Bmatrix} \xi_1 \\ \eta_1 \end{Bmatrix}. \tag{33}$$

Using these forces the SIF, i.e., the stress intensity factor (K_1) for crack 1 can be found from equations (2)–(4) as given below:

$$K_1^I = \frac{Q_{\xi_1} L\alpha'\sqrt{\pi\alpha}F}{8I} + \frac{Q_{\eta_1} Lw\sqrt{\pi\alpha}F'}{4I}. \tag{34}$$

The sign of (K_1^I) at different positions along the crack edge would indicate the open and closed area of crack 1. Positions where the sign is positive correspond to open area of the crack represented by A_1. This enables setting up the limits of integration for crack area A_1. These limits involve both the width and height of the cracked area. Similarly, the forces obtained from equation (33) can be used to estimate the forces Q_{ξ_2} and Q_{η_2} acting on crack 2, by using equation (1). Then the SIF on the edge of crack 2 is determined as follows:

$$K_2^I = \frac{Q_{\xi_2} L\alpha'\sqrt{\pi\alpha}F}{8I} + \frac{Q_{\eta_2} Lw\sqrt{\pi\alpha}F'}{4I}. \tag{35}$$

The sign of SIF K_2^I at various locations on crack 2 indicates open/closed area of crack 2, which helps in setting limits of integration wherever A_2 is involved.

Equation (32) can be non-dimensionalized using the following parameters:

$$\bar{\xi} = \frac{\xi_1}{\delta_{st}}, \quad \bar{\eta} = \frac{\eta_1}{\delta_{st}}, \quad \zeta = \frac{c}{2\sqrt{k_0 m}}, \quad \tau = \omega t, \quad e = \frac{\in}{\delta_{st}}, \quad \bar{a}_1 = \frac{a_1}{D}, \quad \bar{a}_2 = \frac{a_2}{D}. \tag{36a}$$

Also, the following frequency ratios are defined:

$$r_0 = \frac{\omega_0}{\omega}, \quad r_\xi = \frac{\omega_\xi}{\omega}, \quad r_\eta = \frac{\omega_\eta}{\omega}, \quad r_{unb} = \frac{\omega}{\omega_0}, \quad r_{\xi\eta} = \frac{\omega_{\xi\eta}}{\omega}, \quad r_{\eta\xi} = \frac{\omega_{\eta\xi}}{\omega},$$

where

$$\omega_0 = \sqrt{\frac{k_0}{m}}, \quad \omega_\xi = \sqrt{\frac{k_\xi}{m}}, \quad \omega_\eta = \sqrt{\frac{k_\eta}{m}}, \quad \omega_{\xi\eta}\omega_{\eta\xi} = \sqrt{\frac{k_{\xi\eta}}{m}}. \tag{36b}$$

Hence, the equations of motion in non-dimensional form are

$$\ddot{\bar{\xi}} + 2\varsigma r_0\dot{\bar{\xi}} + 2\dot{\bar{\eta}} + (r_\xi^2 - 1)\bar{\xi} + (r_{\xi\eta}^2 - 2\varsigma r_0)\bar{\eta} = e\cos\beta - r_0^2\cos\tau,$$

$$\ddot{\bar{\eta}} + 2\varsigma r_0\dot{\bar{\eta}} + 2\dot{\bar{\xi}} + (r_\eta^2 - 1)\bar{\eta} + (r_{\eta\xi}^2 + 2\varsigma r_0)\bar{\xi} = e\sin\beta + r_0^2\sin\tau. \tag{37}$$

A program has been written in MATLAB® (version 5.3) to estimate the response of a two-crack rotor. The solution process for solving the above equations of motion is

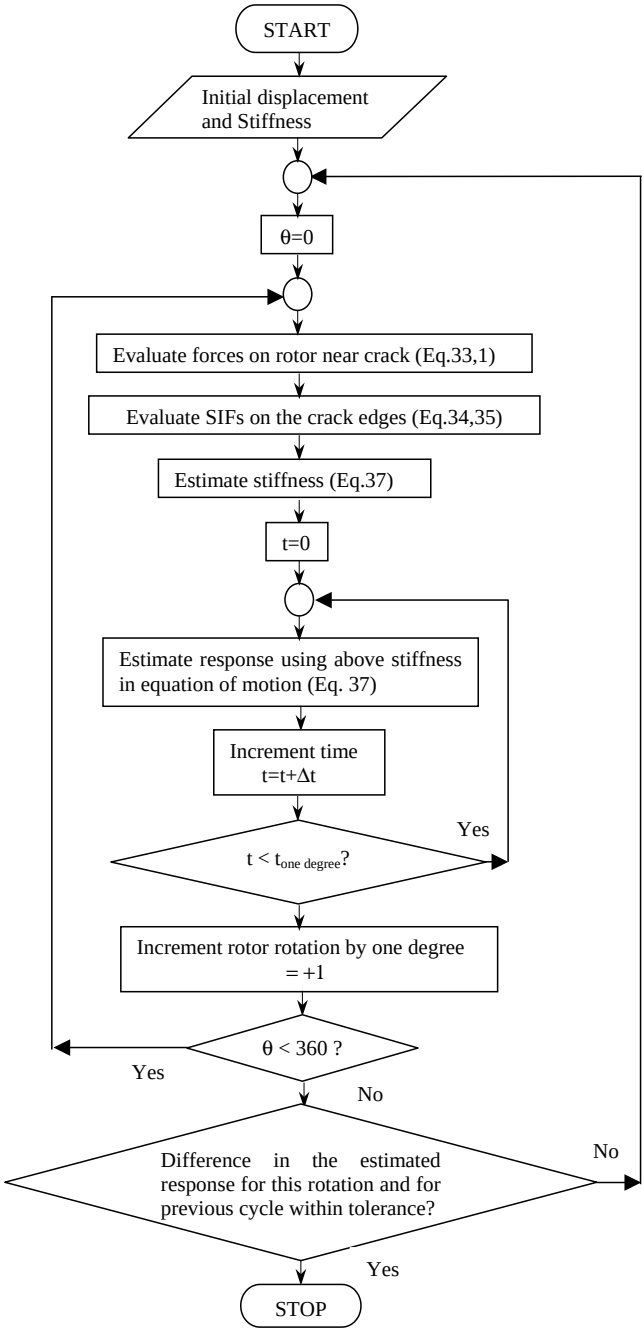

Figure 2. Flowchart showing the procedure of solution of equations of motion.

iterative and is detailed in Figure 2. The initial displacement is assumed equal to the static deflection of the uncracked rotor and initial stiffness values correspond to that of the uncracked rotor. Using these initial displacements and stiffness, the program evaluates forces (Q_ξ and Q_η) on both the crack cross-sections with the help of equations (33) and (1).

Then using these forces and equations (34) and (35), SIF at 50 points along the crack edge of both the cracks are evaluated. Positive SIF values indicate the amount of open part of the crack. This in turn decides the limits of integration for equations (30) since only the open part of the crack is taken into account for finding the additional flexibility due to the cracks. The flexibility values are calculated from equations (27)–(29) which give stiffnesses using equation (31). Then, equation (37) is integrated using fourth order Runge–Kutta procedure using the initial assumed response and stiffnesses. Stiffnesses are assumed to be constant for one degree of rotation ($\pi/180$ radian), for which the integration of equation (37) is carried out with a sufficiently small time step ($\Delta t = 0{\cdot}00001445$ s). The response obtained at the end of one degree of rotation is stored and again used to re-evaluate forces using equation (33). These forces are used to evaluate the SIF and the next set of stiffness values that are used in equation of motion to get next set of displacements (ξ_1 and η_1). Thus, the response is used to evaluate stiffnesses which in turn give the next set of response. To attain a steady state, the iterative procedure is repeated till the response set for one full rotation is converged. The tolerance for convergence of response in the present case is taken to be of the order of 0·1%. Initial transients in the response die within the first few rotor rotations. Steady state solution is obtained after that.

At each solution step, the SIF values at all the 50 locations along the edges of both the cracks are evaluated. Using the sign of these SIF values the crack closure line position (CCLP) is found. The CCLP essentially separates the open and closed area of the crack. The CCLP for both the cracks is stored during each solution step. This helps in understanding the breathing behaviour of the two cracks as the position of the line shows how the cracks close and open. The significance of CCLP is shown in Figure 3. The crack edge is shown as A–B whereas the crack closure line (CCL) denoted by a bold vertical line perpendicular to the crack edge is also shown. The position of CCL keeps changing along the crack edge (say from 1 to 50 while opening from A to B and from 50 to 100 while closing from A to B) as the rotor rotates. When the rotor is at initial position (Figure 3(a)), the crack edge is on the compression region and is closed completely under the action of gravity. As the rotor starts rotating counterclockwise, part of the crack near end "A" opens up. Thus at any position say $\theta = 45^\circ$, the CCL could be at point 15 along the crack edge (Figure 3(b)). When the rotor rotates further and when the crack edge is vertical at $\theta = 90^\circ$, the CCL could be at position 25 along the crack edge (Figure 3(c)) and so on. The crack edge opens fully when it comes on the lower side in the tensile region at around $\theta = 180^\circ$ (Figure 3(e)). At this position, the CCL has travelled from one corner A to the other corner B passing through 50 various points along the crack edge and the CCL position keeps changing from 0 to 50. When the rotor rotates further the corner A starts to close and the CCL position changes from 50 towards 100 as the crack begins to further close from corner A to B (Figures 3(f)–3(h)) till the crack completely closes at around $\theta = 360^\circ$. Thus the CCL position of 1 and 100 indicates a fully closed state, whereas CCLP of 50 indicates a fully open crack state. CCLP of 25 indicates half open-half closed condition and CCLP of 75 indicates half closed-half open state of crack. Thus the CCL position is indicative of the breathing of the crack.

3. ROTOR WITH TWO BREATHING CRACKS

To validate the two-crack model developed in section 2, a simulation involving two cracks with $\bar{a}_1 = 0{\cdot}04$ and $\bar{a}_2 = 0{\cdot}005$ is considered. The angle between them is assumed to be $\gamma = 0^\circ$. This is to compare the unbalance response of the two-crack rotor with similar response of a cracked rotor with a single transverse crack of depth $\bar{a} = 0{\cdot}4$ presented in

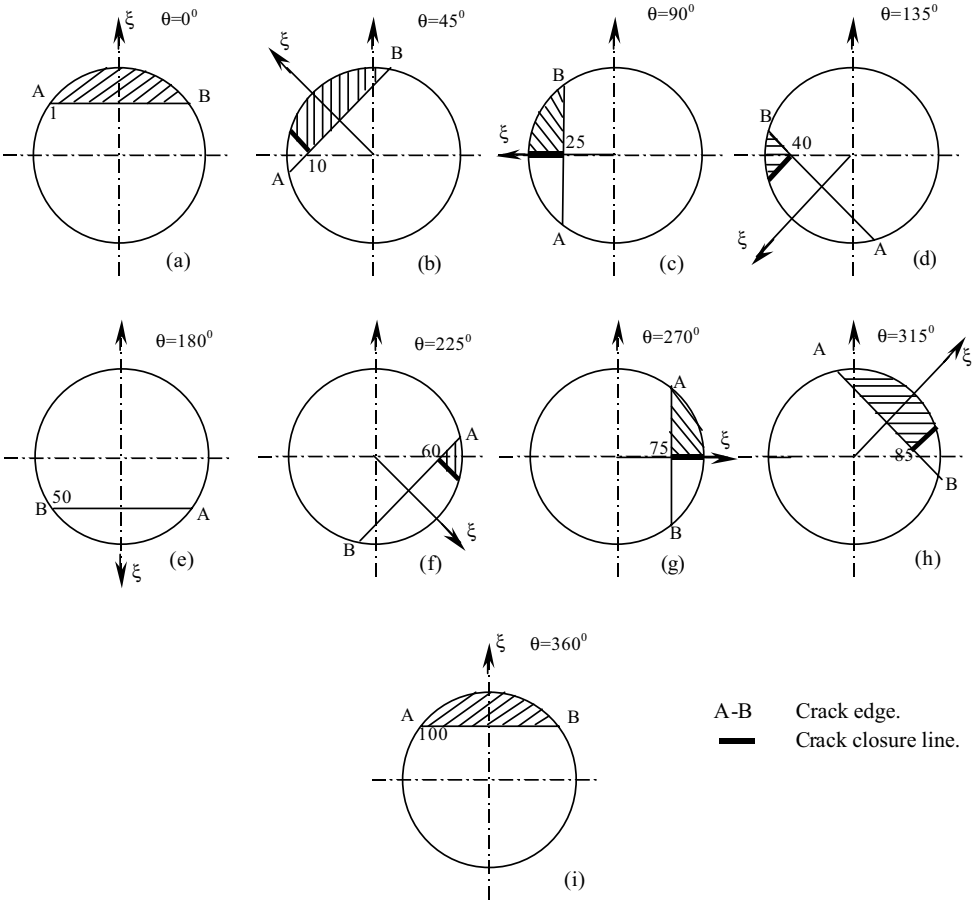

Figure 3. Variation of crack closure line position with angular position of rotor.

reference [10]. The depth ratio of $\bar{a}_2 = 0{\cdot}005$ is not expected to change the response of the two-crack rotor while at the same time it will allow the validation of the new model. The unbalance eccentricity and the rotational speed considered are $e = 0{\cdot}1$ and $r_{unb} = 0{\cdot}5$ respectively. Unless otherwise stated, the unbalance orientation angle β is assumed to be 0° in all the simulations of this paper.

The results obtained by the two-crack rotor model are presented in Figure 4. Figure 4(a) shows variation of the direct stiffness ratios (k_ξ/k_0 and k_η/k_0) whereas Figure 4(b) shows variation of cross-coupled stiffness ratio (k_η/k_0). Similarly Figures 4(c) and 4(d) show the unbalance response in rotor fixed and stationary co-ordinate systems respectively. These results are in accordance with the results presented in reference [11]. The direct stiffness ratios k_ξ/k_0 indicating stiffness variation in the ξ direction varies between 0·9084 and 1 whereas similar ratio in the η direction (k_η/k_0) varies between 0·9595 and 1. Both the stiffness values drop to their minimum near $\theta = 180^\circ$, where the crack usually opens fully. The cross-coupled stiffness is however zero near $\theta = 180^\circ$ and maximum near $\theta = 90^\circ$ and 270° when the crack is half-closed–half-open. The response in Figure 4(d) clearly shows predominant $2x$ harmonic component in both horizontal and vertical directions. This is due to the fact that the rotational speed is equal to 1/2 the bending critical speed corresponding to the uncracked rotor.

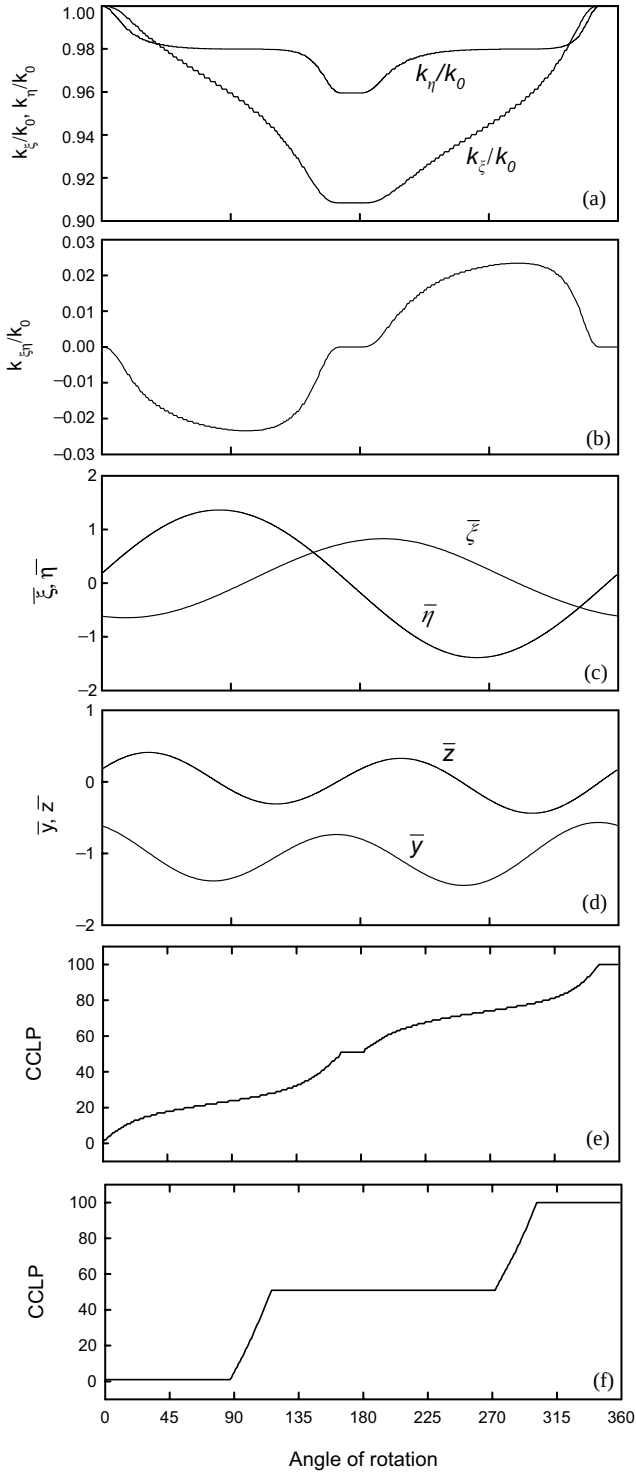

Figure 4. Response of a two-crack rotor with $\bar{a}_1 = 0{\cdot}4$, $\bar{a}_2 = 0{\cdot}05$, $r_{unb} = 0{\cdot}5$ and $\gamma = 0^\circ$. (a) Direct stiffness ratio variation with rotation. (b) Cross-coupled stiffness ratio variation. (c) Response in rotor-fixed co-ordinates. (d) Response in stationary co-ordinates. (e) Crack closure line position (CCLP) variation for crack 1. (f) CCLP variation for crack 2.

Figures 4(e) and 4(f) show crack closure line position (CCLP) for cracks 1 and 2 as the two-crack rotor completes one resolution. The CCLP is explained in Figure 3. Figure 4(e) shows that the crack 1 opens immediately and gradually keeps opening up until it opens completely near $\theta = 160^\circ$. From $\theta = 180^\circ$ onwards it starts closing again and it closes completely just before $\theta = 360^\circ$. However for crack 2 (Figure 4(f)) which is a very shallow crack, the crack remains closed for a considerable period (till $\theta = 90^\circ$) after which it starts opening rather quickly and opens completely at $\theta = 120^\circ$. It stays open for a considerable time before it starts closing again at 270° and closes very quickly. This is in contrast to the breathing of crack 1, which shows a more gradual opening and closing. This also indicates that the sudden open (at $\theta = 90^\circ$) and sudden close (at $\theta = 270^\circ$) mechanism suggested by Grabowski [14] indeed is seen here for crack 2. However this applies for very shallow cracks and cannot be generalized to all the crack depths. Similarly, from Figure 4(a) it may be noted that the stiffness variation is not actually sinusoidal for the cracked rotor as suggested by Mayes and Davis [15]. However it is still a reasonable approximation.

Next, the effect of one crack with a reasonable depth on a similar crack located at an angle γ with respect to the first one is studied. The rotor speed considered is $r_{unb} = 0{\cdot}1$ and two equal cracks with $\bar{a}_1 = \bar{a}_2 = 0{\cdot}2$ are considered. The results of the simulation are shown in Figure 5 with $\gamma = 0^\circ$ (Figure 5(I)) and $\gamma = 45^\circ$ Figure 5(II)). Figures 5(a) and 5(b) show direct and cross-coupled stiffness variation for one cycle of rotation for $\gamma = 0^\circ$. The direct stiffness k_ξ drops to minimum value near $\theta = 135^\circ$ from $k_\xi/k_0 = 1$ to 0·9645 whereas the other direct stiffness k_η drops from $k_\eta/k_0 = 1$ to 0·9944. The cross-coupled stiffness is also to have a maximum value near $\theta = 270^\circ$ and a minimum at $\theta = 90^\circ$ while the stiffness is zero at $\theta = 180^\circ$. Figures 5(c) and 5(d) shows the time domain response in vertical and horizontal directions. The substantial dip in the rotor response near $\theta = 180^\circ$ is clearly seen in Figure 5(c) which is related to the fully opened crack in the range of $\theta = 135-225^\circ$ under the influence of gravity. From Figures 5(e) and 5(f) it may be noted that both the cracks start to open at about $\theta = 40^\circ$ and open fully near $\theta = 135^\circ$. Both the cracks start to close again as shown by the CCLP changing from position 50 to 100 after $\theta = 225^\circ$. This breathing of both the cracks is synchronous which is expected because they are aligned. When the orientation of crack 2 is changed from $\gamma = 0$ to 45° with respect to crack 1, the effect on the stiffness variation is evident. In the case of $\gamma = 45^\circ$, the overall stiffness drop in the ξ direction is reduced with corresponding increase in the drop of stiffness in the η direction (Figure 5(g)), as compared with the case of the two cracks aligned together (Figure 5(a)). The cross-coupled stiffness also shows an increase in the change of stiffness value for $\gamma = 45^\circ$. The effect of these stiffness changes is seen on the response shown in Figures 5(c), 5(d), 5(i) and 5(j). Although there is no significant qualitative changes in the vertical and horizontal response from $\gamma = 0$ and 45°, the peak response shows a certain drop in the amplitudes (Figures 5(i) and 5(j)). Both these cracks, when they are aligned, open and close at identical position, which is quite obvious (Figures 5(e) and 5(f). However, when the orientation changes to $\gamma = 45^\circ$, crack 2 opens in advance compared to crack 1 because of the counterclockwise rotation of the rotor (Figures 5(k) and 5(l)). This is in fact effecting the typical stiffness variation shown in Figures 5(g) and 5(h). The simulation results presented here in Figure 5 show noticeable effect of the orientation of the two cracks on the response and stiffness variation pattern of the two-crack rotor.

When the orientation angle of the crack 2 is increased from $\gamma = 45$ to 90°, there are substantial changes observed in stiffness variation as well as the response (Figures 6(a)–6(f)). With $\gamma = 90^\circ$, the drop in stiffness in both ξ and η directions is by equal amount (Figure 5(a)) which is expected because of the fact that the two equal cracks are perpendicular to each other. The peak response level in both directions has dropped by

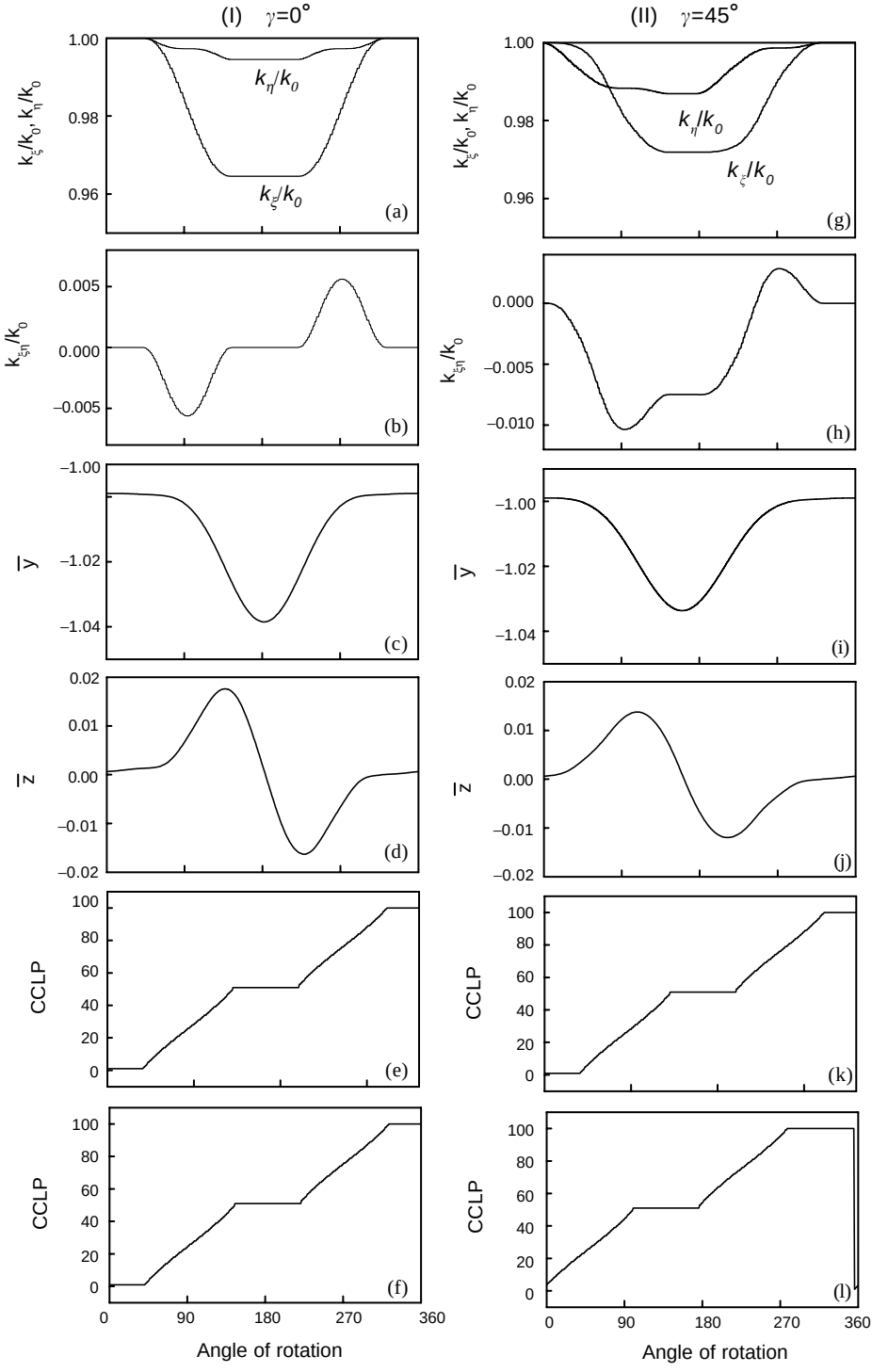

Figure 5. Response of a two-crack rotor with $\bar{a}_1 = 0{\cdot}2$, $\bar{a}_2 = 0{\cdot}2$, $r_{unb} = 0{\cdot}1$. (I) $\gamma = 0^\circ$. (II) $\gamma = 45^\circ$. (a) Direct stiffness ratio variation with rotation. (b) Cross-coupled stiffness ratio variation. (c) Lateral vertical response. (d) Lateral horizontal response. (e) Crack closure line position (CCLP) variation for crack 1. (f) CCLP variation for crack 2.

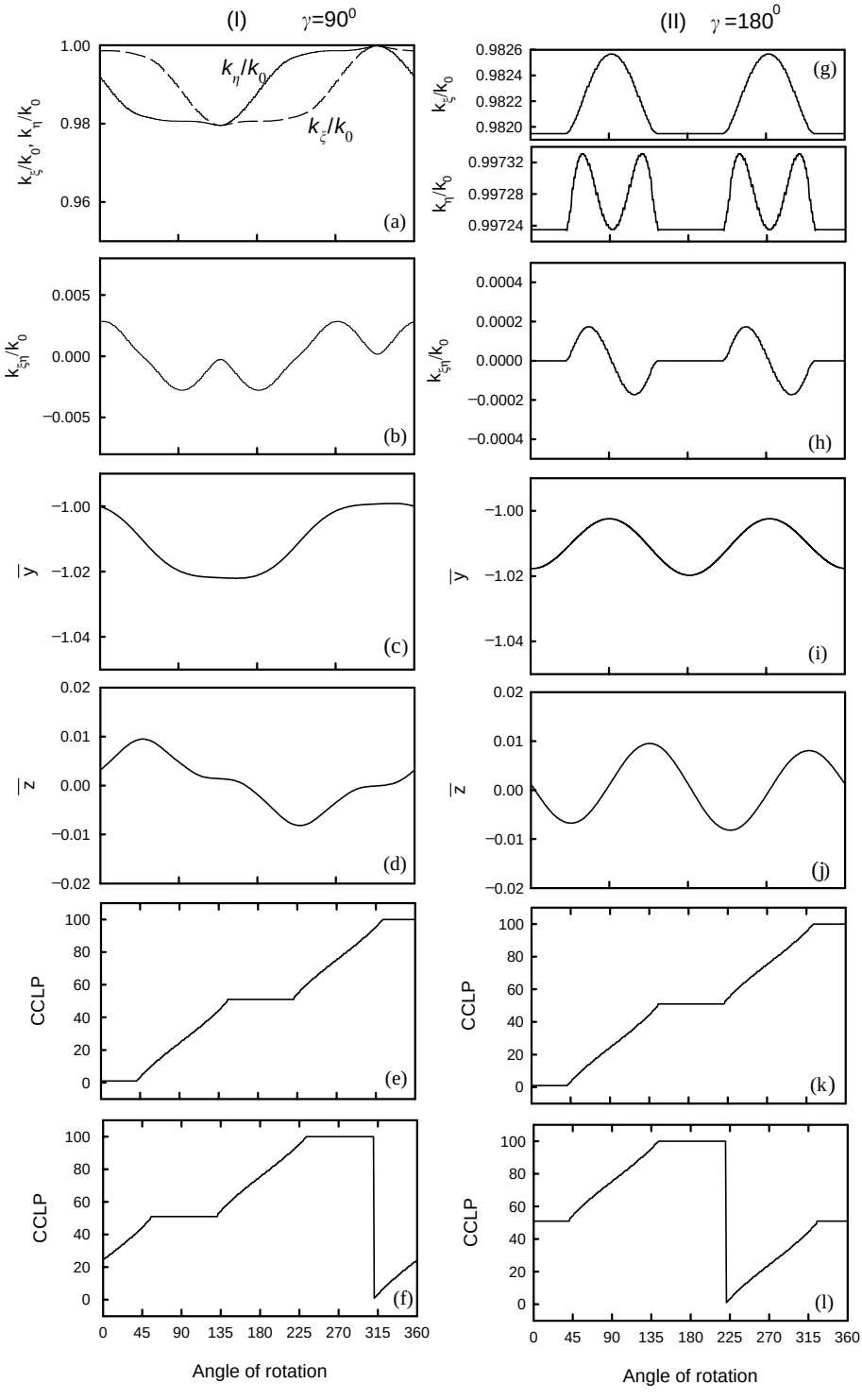

Figure 6. Response of a two-crack rotor with $\bar{a}_1 = 0{\cdot}2$, $\bar{a}_2 = 0{\cdot}2$, $r_{unb} = 0{\cdot}1$. (I) $\gamma = 90^\circ$. (II) $\gamma = 180^\circ$. (a) Direct stiffness ratio variation with rotation. (b) Cross-coupled stiffness ratio variation. (c) Lateral vertical response. (d) Lateral horizontal response. (e) Crack closure line position (CCLP) variation for crack 1. (f) CCLP variation for crack 2.

almost 50% (Figures 5(c) and 5(d)). The response pattern is also changed when compared with the response at $\gamma = 0^\circ$. The crack opening and closing shows an interesting variation. When the rotor starts turning from $\theta = 0^\circ$, crack 1 starts to open at $\theta = 40^\circ$ and fully opens at $\theta = 150^\circ$ (Figure 6(e)). It then starts closing at $\theta = 225^\circ$ and fully closes near $\theta = 315^\circ$. Whereas crack 2, which is at $\gamma = 90^\circ$ with respect to crack 1, is already half-open at $\theta = 0^\circ$ (Figure 6(f)) and continues to open till it opens fully at $\theta = 45^\circ$, remains open till $\theta = 135^\circ$ and then starts to close. It closes completely at $\theta = 225^\circ$ and starts to open again at $\theta = 315^\circ$. When open–close pattern of both the cracks is considered, it may be noted (from the CCLP in Figures 6(e) and 6(f)) that when one crack is fully closed or fully open the other is partially open. This has a definite effect on the response of the two-crack rotor that is discussed with the help of frequency domain and orbit plots in the following paragraphs. But before that an interesting case of $\gamma = 180^\circ$ is considered. When $\gamma = 180^\circ$, the two cracks are opposite to each other in their orientation on the rotor. Effectively this causes a strong asymmetry in the rotor stiffness. This is evident in Figure 6(g), wherein the two direct stiffness ratio variations show negligible variation about their mean values. In fact the stiffness ratio variation is a straight line if shown in the same limits as in Figure 6(a). This strong asymmetry shows its effect in the lateral rotor vibration response as shown in Figures 6(i) and 6(j). The response shows a very strong 2nd harmonic component in both the directions (y and z). The stiffness asymmetry of the rotor is also indicated in Figures 6(k) and 6(l), wherein if crack 1 is closed fully at $\theta \geqslant 315^\circ$ and at $\theta \leqslant 45^\circ$, the crack 2 is open fully in this range. Similarly when one crack starts to close from fully open state, the other crack starts to open from fully closed state and *vice versa*. This maintains the overall stiffness in the two directions nearly constant leading to the condition of a slotted rotor.

The interaction between two cracks oriented at an angle with respect to each other has been shown to effect the stiffness variation and also the response in the foregoing discussions. The effect on the response is now discussed with the help of frequency domain signals and the orbit plots. Figures 7(I), 7(II) and 7(III) show the response with $\gamma = 0$, 90 and 180° respectively. When $\gamma = 0^\circ$, the vertical rotor response (Figure 7(c)) shows first, second and third harmonics of rotational frequency (4·27 Hz) in decreasing levels of amplitudes. In the horizontal vibration spectrum (Figure 7(d)) the first two harmonics are equal and the third harmonic is relatively weak. The orbit shape in this case is onion shaped (Figure 7(e)). When $\gamma = 90^\circ$, frequency composition of the response dramatically changes. Now both the vertical (Figure 7(h)) and horizontal (Figure 7(i)) vibration spectra show only first and third harmonic components without any second harmonic component. The first harmonic is twice as strong in vertical direction than in the horizontal direction whereas the third harmonic is much stronger in the horizontal direction than in the vertical direction. The orbit is slightly changed here (Figure 7(j)); being symmetric about both y and z directions and reduced considerably in size. When $\gamma = 180^\circ$, again there are dramatic changes in the spectra. In this case the strong stiffness asymmetry shows up in the form of predominant $2x$ component with almost negligible $1x$ and no trace of third harmonic in both the vertical and horizontal spectra (Figures 7(m) and 7(n)). Obviously, the orbit plot is a double looped orbit here (Figure 7(o)).

The simulation is repeated at a higher speed of $r_{unb} = 0{\cdot}5$. The response in time and frequency domain for the three cases of γ (0, 90, 180°) is shown in Figure 8. It may be noted that the response changes substantially when γ is changed from 0 to 90°. The strong second harmonic component of vibration earlier seen in the case of $\gamma = 0^\circ$ almost disappears and the double looped orbit reduces to an oblong orbit (Figure 8(j)). This is because in the case of $\gamma = 90^\circ$, the overall stiffness variation in both directions is dominant as seen from the frequency domain signal (Figures 8(h) and 8(i)). However, the response is

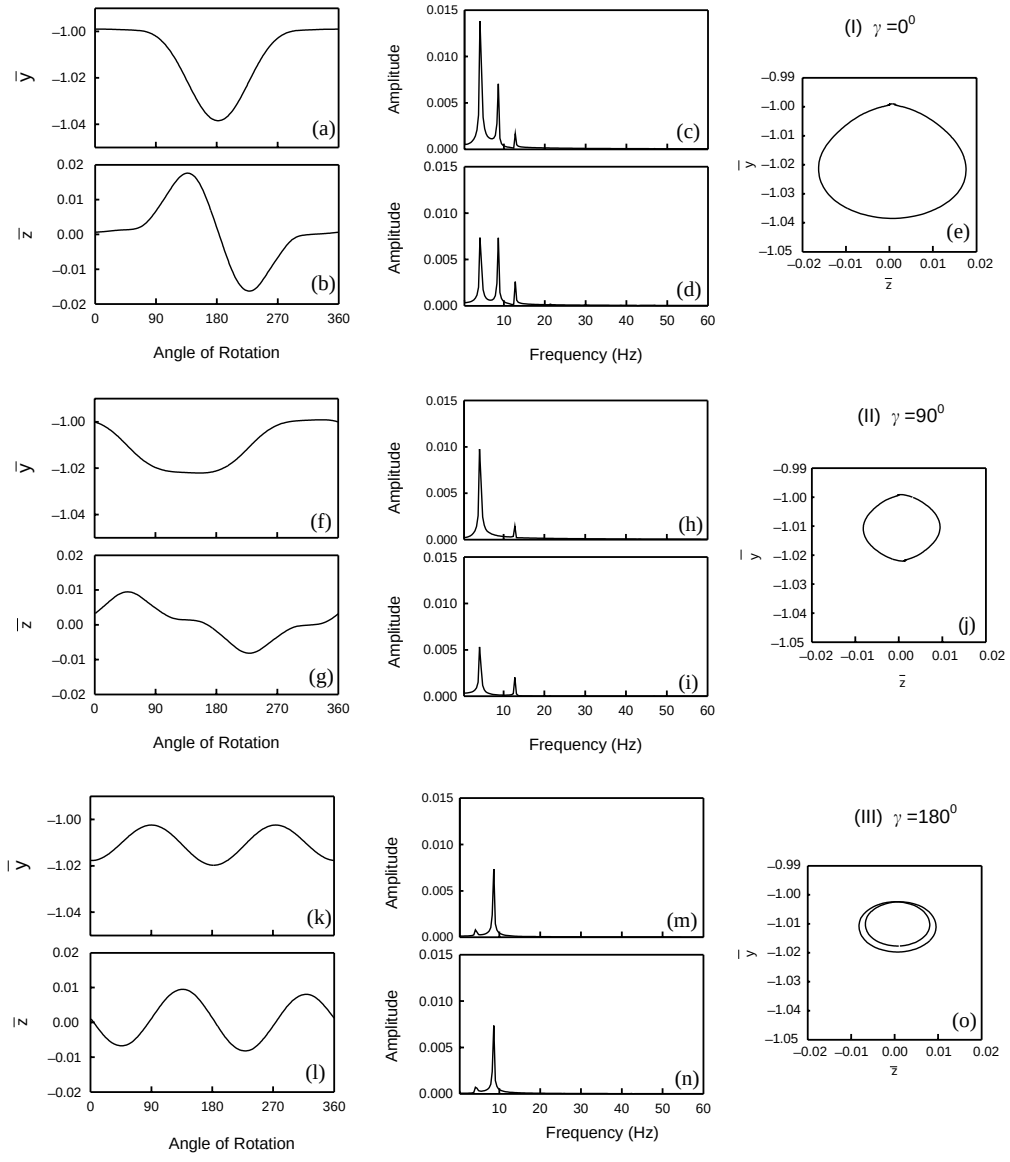

Figure 7. Response of a two-crack rotor with $\bar{a}_1 = 0{\cdot}2$, $\bar{a}_2 = 0{\cdot}2$, $r_{unb} = 0{\cdot}1$. (I) $\gamma = 0^\circ$. (II) $\gamma = 90^\circ$. (II) $\gamma = 180^\circ$. (a) Time domain response in vertical direction. (b) Time domain response in horizontal direction. (c) Frequency domain response in vertical direction. (d) Frequency domain response in horizontal direction. (e) orbit plot.

similar for $\gamma = 0$ and 180°. When the simulation is repeated for even higher speed of $r_{unb} = 0{\cdot}8$, it is found that the response does not change in any way when the orientation of a crack is changed with respect to the other. This is due to the fact that at such a high speed close to critical speed, the response due to flexibility dominates the overall unbalance response and the stiffness asymmetry or the stiffness variation plays a very little role. It should be emphasized that the crack effect in the form of higher harmonics is more clearly observed at a lower speed than at a higher speed.

The effect of unbalance orientation angle (β) relative to the crack 1 on the response of the two-crack rotor is also studied. To investigate the influence of β, the response of the

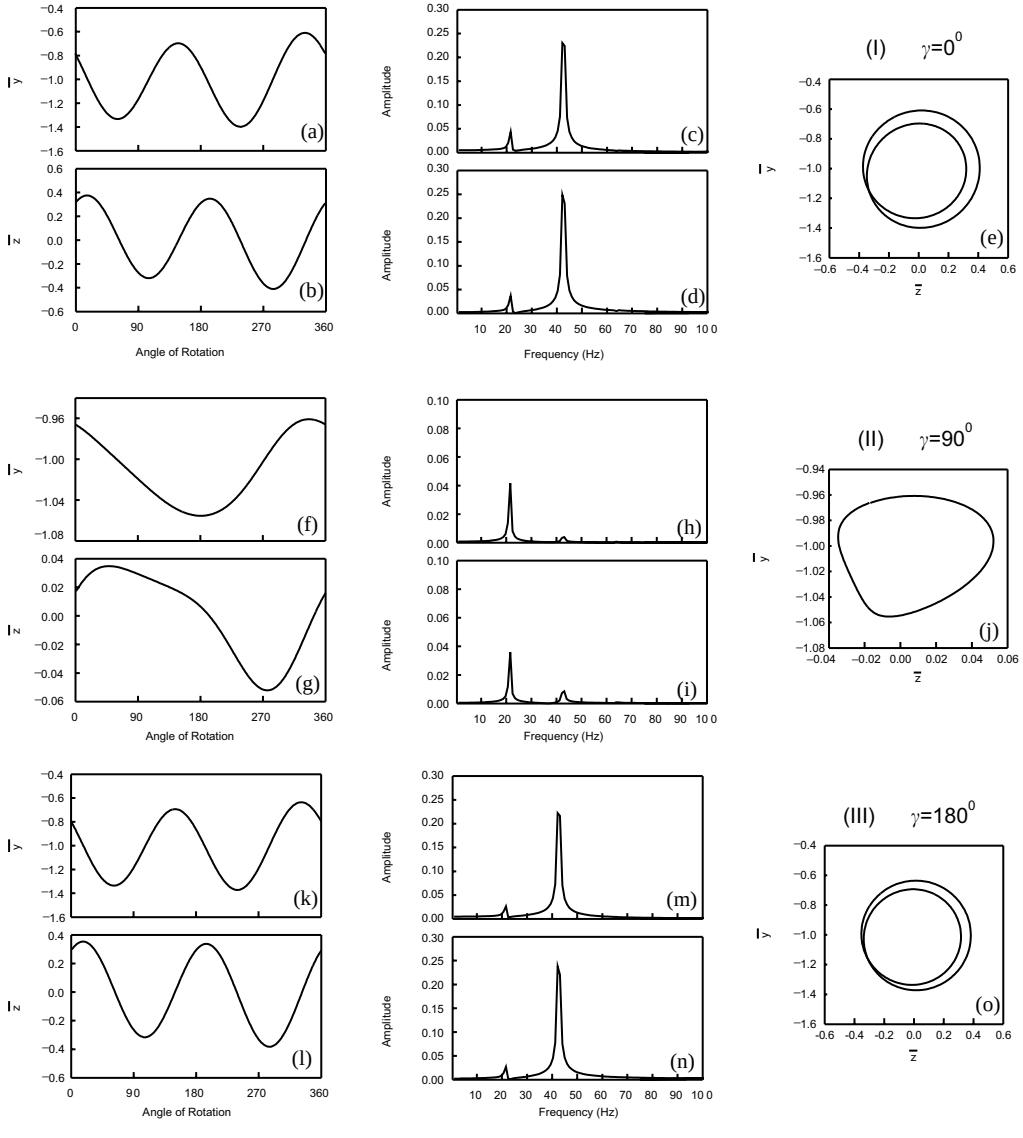

Figure 8. Response of a two-crack rotor with $\bar{a}_1 = 0{\cdot}2$, $\bar{a}_2 = 0{\cdot}2$, $r_{unb} = 0{\cdot}5$. (I) $\gamma = 0^\circ$. (II) $\gamma = 90^\circ$. (II) $\gamma = 180^\circ$. (a) Time domain response in vertical direction. (b) Time domain response in horizontal direction. (c) Frequency domain response in vertical direction. (d) Frequency domain response in horizontal direction. (e) orbit plot.

two-crack rotor is obtained by varying the value of β from 0 to 360° in step of 90°. The speed of rotor for these simulations is kept as 1/2 of the first bending critical speed. The effect of β is shown in Figure 9 in which the response variation with β is shown for three different crack orientation angles (γ), namely 0, 90 and 180°. Noticeable variation for all the three cases of γ is observed. The variation of orbit shape with β for $\gamma = 0^\circ$ obtained here (Figure 9(a)) is similar to that presented in reference [11] for the case of single crack. The variation of orbit shape with β is similar for $\gamma = 0$ and 180°. For both these cases the frequency pattern (the spectra not shown here) did not show any significant changes. However when the unbalance is opposite to the crack ($\beta = 180^\circ$), the amplitude of the first harmonic reduces and the two loops of the orbit plot are almost of the same size. This is in

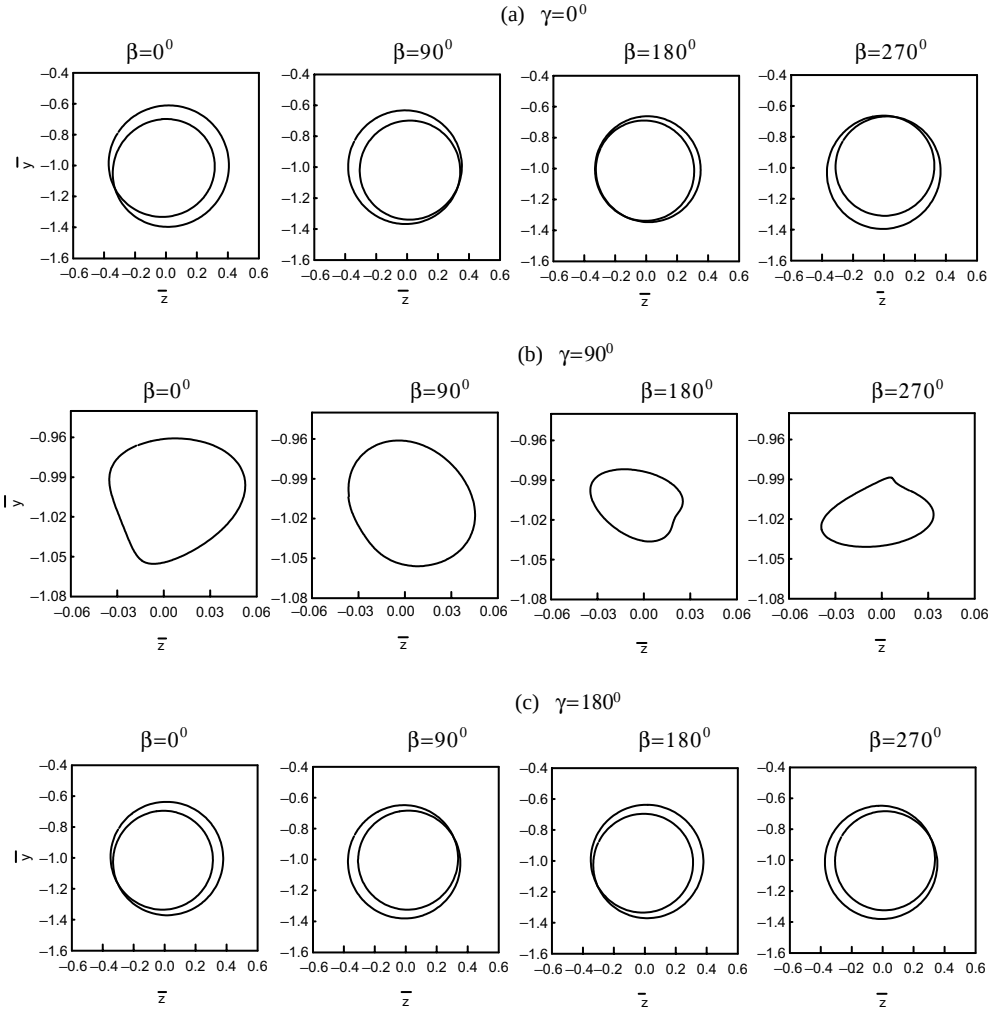

Figure 9. Effect of unbalance orientation angle (β) on the orbital response of a two-crack rotor with $\bar{a}_1 = 0{\cdot}2$, $\bar{a}_2 = 0{\cdot}2$, $r_{unb} = 0{\cdot}5$. (a) $\gamma = 0^\circ$. (b) $\gamma = 90^\circ$. (c) $\gamma = 180^\circ$.

contrast to the case of $\beta = 0^\circ$ where the outer loop is a little larger than the inner loop. The relative sizes of inner and outer loops are similar for $\beta = 90$ and 270°. The second harmonic component in all the four cases of β is not affected by the value of β. For $\gamma = 90^\circ$, the first harmonic component substantially reduces for $\beta = 180$ and 270°, since for these values the unbalance is effectively in opposite phase to the crack. Thus the orbit plot in this case (Figure 9(c)) can be seen as reduced in size. However it may be noted that for each value of β, the effect of crack orientation angle γ on the response of the two-crack rotor that is discussed earlier in the section is seen to be similar in nature.

4. ROTOR WITH ONE OPEN AND ONE BREATHING CRACK

A special case of the two-crack rotor is an asymmetric rotor with a single breathing transverse crack at an orientation γ. This is like one of the two cracks is constrained to

remain always open and the other crack breathe and change its stiffness as the rotor rotates. The program written for the two-crack rotor is modified so that crack 1 is always open and thus represents the constant stiffness asymmetry of an asymmetric rotor in rotor fixed co-ordinates. The other crack, crack 2 is allowed to breathe and it may represent a transverse crack in an asymmetric rotor. Such cracks are often found in two pole generator rotors and are known to occur at the roots of winding slots due to stress concentrations and thermal gradients due to electrical windings. It would be interesting to study the effect of the presence of such a transverse surface crack on the dynamics of an asymmetric rotor.

Before the effect of a crack on an asymmetric rotor is studied, the authors have found the response of an asymmetric rotor (without any crack) using a program that is separately developed. This is expected to help in understanding the additional effect the crack would bring about in the already existing inherent stiffness asymmetry of the asymmetric rotor. Figure 9(I) shows the response of an asymmetric rotor at $r_{unb} = 0{\cdot}1$ with an asymmetry corresponding to a crack of depth $\bar{a} = 0{\cdot}2$. The time domain (Figures 9(a) and 9(b)) and the frequency domain (Figures 9(c) and 9(d)) responses as expected show a very dominant second harmonic vibration component to an extent that the first harmonic component is almost absent. This is because the speed being very low, the effect of unbalance is negligible compared to the effect of stiffness asymmetry. The stiffness in rotating co-ordinates being constant in case of an asymmetric rotor, the stiffness ratio is a straight line if Figure 9(e). The orbit plot here is a double loop orbit with both loops being almost of the same size.

Next, a breathing crack is introduced in addition to the constant asymmetry of the asymmetric rotor. Figure 9(II) shows the response of an asymmetric rotor with a transverse crack at an orientation of $\gamma = 0^\circ$. The time domain response (Figures 9(g) and 9(h)) shows a noticeable change. The frequency domain signal (Figures 9(i) and 9(j)) clearly shows a drop in $2x$ vibration component and a substantial increase in $1x$ vibration component in addition to the traces of higher harmonics ($3x$) typical of the presence of a crack. The stiffness ratio k_ξ/k_0 drops from a value of 0·9819 corresponding to the constant stiffness of the asymmetric rotor to a value of 0·9645 due to an increased flexibility owing to the present of the crack. This drop takes place when the crack opens fully ($\theta = 135^\circ - 225^\circ$). Such a drop in flexibility during a part of the rotation leads to a typical orbit as shown in Figure 9(l). Though the orbit has a loop inside similar to the one in the case of asymmetric shaft in Figure 9(f), the difference is quite clear. The inner loop is quite small and together with the larger outer lobe, the orbit takes this shape because of the increased $1x$ component due to additional flexibility due to the crack. The effect of the additional presence of the crack is thus very clearly seen in the frequency domain and in the orbit plot of the response.

When the orientation of the crack from the direction of asymmetry is changed from $\gamma = 0$ to 45°, the effect is seen in the orbit plot more prominently than in the other format. Although the frequency spectra and time domain signals show no qualitative changes from the earlier case of $\gamma = 0^\circ$, the orbit plot (Figure 9(r)) shows a clear shift in the orbit orientation. Due to an increased orientation angle the drop in stiffness ratio (Figure 9(q)) is increased for k_η/k_0 and decreased for k_ξ/k_0. When the orientation of crack is further increased to $\gamma = 90^\circ$, the marked drop in the degree of asymmetry compared to previous cases of γ is observed in the time domain, (Figures 10(a) and 10(b)) and frequency domain (Figures 10(c) and 10(d)) signals. The time domain signal shows a strong qualitative change. The strong $2x$ harmonic component in time domain signal is quite suppressed here. This is also evident from the orbit plot (Figure 10(f)) that shows a complete disappearance of the inner loop that is such a strong feature of an asymmetric rotor at

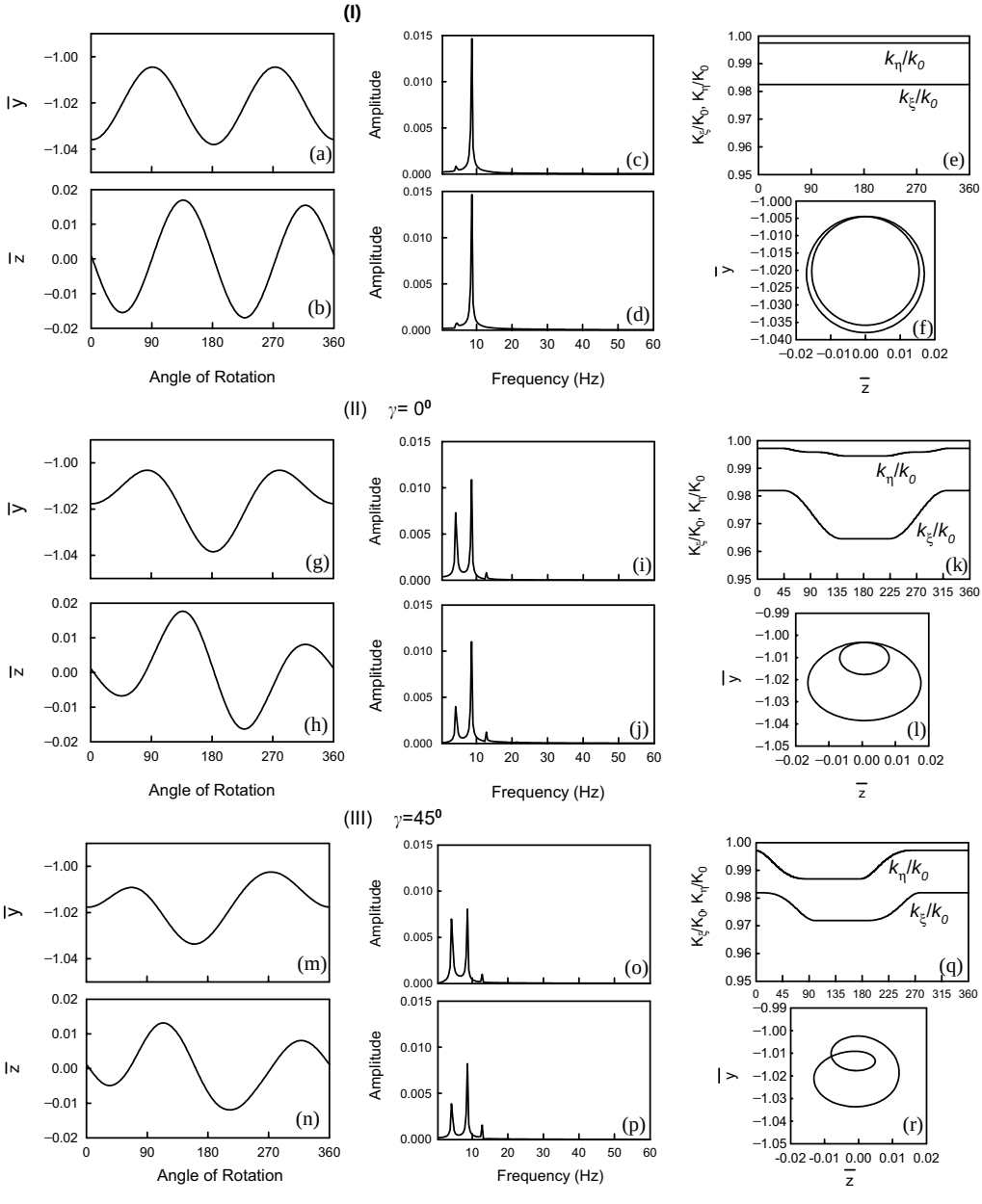

Figure 10. Response of a two-crack rotor with $\bar{a}_1 = 0{\cdot}2$, $\bar{a}_2 = 0{\cdot}2$, $r_{unb} = 0{\cdot}1$. (I) Asymmetric rotor without crack; (II) Asymmetric rotor with crack at $\gamma = 0^\circ$; (III) Asymmetric rotor with crack at $\gamma = 45^\circ$. (a) and (b) Time domain response in vertical and horizontal directions respectively. (c) and (d) Frequency domain response in vertical and horizontal directions respectively. (e) Stiffness ratio variation. (f) Orbit plot.

low speeds. Instead a small protrusion type outer lobe is seen in the orbit plot. Dominating $1x$ component of vibration due to flexibility of the crack reduces the effect of asymmetry due to the asymmetric rotor. The stiffness variation in Figure 10(e) shows that the stiffness ratio k_ξ/k_0 does not change much. This is due to the fact that the constant asymmetry is in the direction of ξ_1 and the additional flexibility induced in ξ_1 direction due to the crack in

$\xi_2-\eta_2$ co-ordinate is very small, ξ_1 being the "strong" crack direction of crack 2. However, the rotor's stiffness in η_1 direction in the early part of the rotation is already reduced due to the orientation of the crack in the η_1 direction (the ξ_2 direction for crack 2 is same as the η_1 direction for crack 1 in this case). The direct stiffness in "weak" crack direction ξ_2 now contributes to the stiffness of the rotor in the η_1 direction, thereby reducing the stiffness of the rotor in the early part of the rotor rotation ($\theta = 45-160^\circ$).

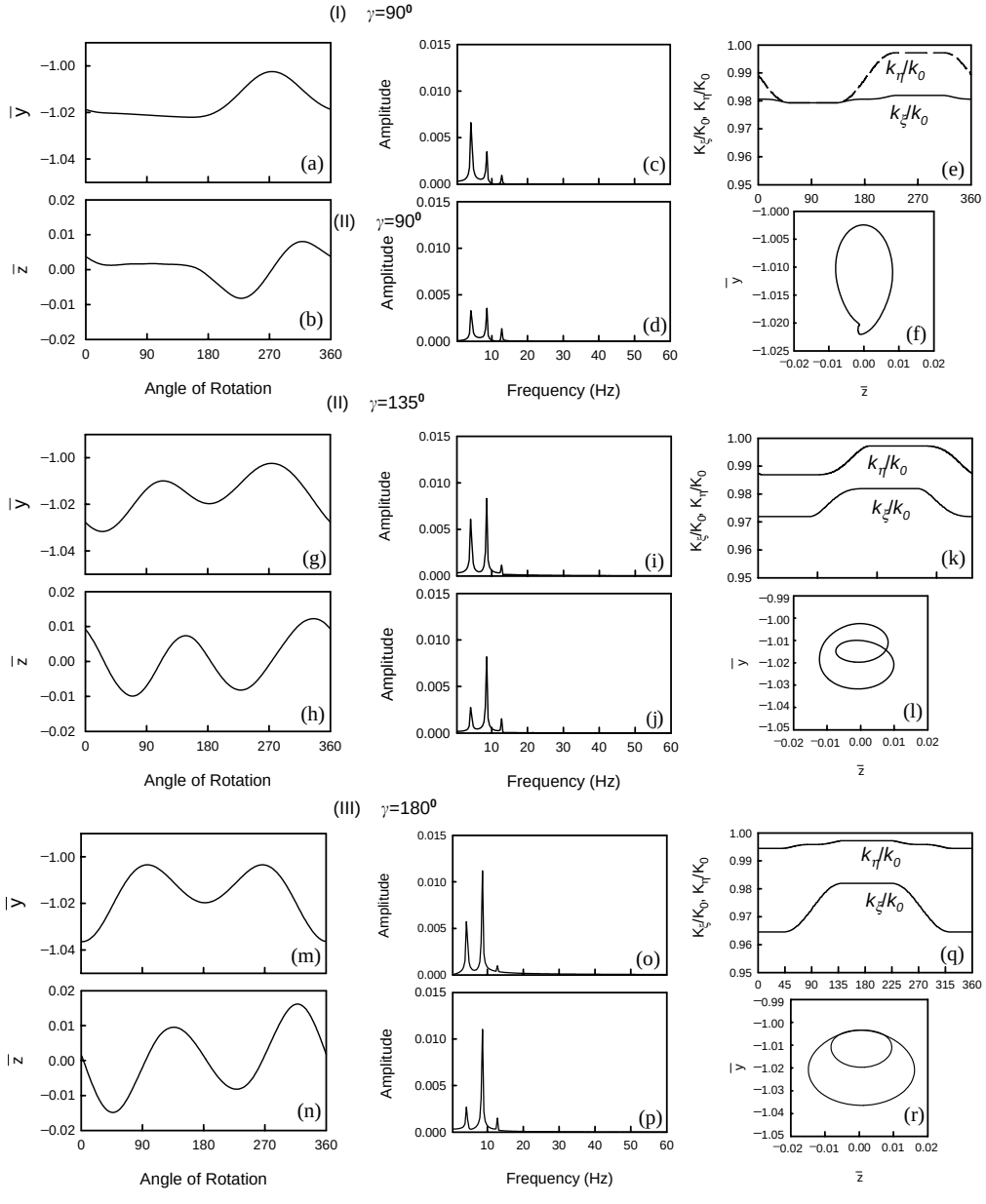

Figure 11. Response of a two-crack rotor with $\bar{a}_1 = 0{\cdot}2$, $\bar{a}_2 = 0{\cdot}2$, $r_{unb} = 0{\cdot}1$. (I) Asymmetric rotor with crack at $\gamma = 90^\circ$; (II) Asymmetric rotor with crack at $\gamma = 135^\circ$; (III) Asymmetric rotor with crack at $\gamma = 180^\circ$. (a) and (b) Time domain response in vertical and horizontal directions respectively. (c) and (d) Frequency domain response in vertical and horizontal directions respectively. (e) Stiffness ratio variation. (f) Orbit plot.

When the orientation angle is further increased to $\gamma = 135^\circ$, the response is similar to the case where $\gamma = 45^\circ$. However, here the orbit plot shows the orbit changed to opposite orientation compared to the case of $\gamma = 45^\circ$. The change in the orbit orientation here clearly emphasizes the need to use plot as none of the time domain or frequency domain plots showed any significant changes in the response.

The case of $\gamma = 180^\circ$ is considered next (Figure 10(III)). Here the time domain and frequency domain signals (Figures 10(m)–10(p)) show an expected rise in the second harmonic vibration component. The stiffness ratio variation (Figure 10(q)) shows an important reversal of pattern. Here since the crack is oriented opposite to the direction of asymmetry, for $\theta = 0^\circ$, the crack is fully open as it is located on the lower side of the rotor in the tensile region. Hence it may be noted that the k_ξ/k_0 ratio is lowest at $\theta = 0^\circ$ and it remains so till the crack on the lower part of the rotor starts to close near $\theta = 80^\circ$, as the rotor continues to rotate counterclockwise. Near $\theta = 135^\circ$, the crack closes and the rotor assumes the stiffness corresponding to the inherent asymmetry in the rotor. Similarly, the orbit shape and orientation of the inner loop in each case of the crack orientation angle γ considered so far does indicate the possible orientation of the crack relative to the direction of asymmetry.

From the foregoing discussions it is established that the presence of a crack in an asymmetric rotor does bring about definite changes in the response of the uncracked asymmetric rotor. The frequency domain response coupled with the orbit plots does provide important information regarding the presence as well as orientation of the crack with respect to the direction of the asymmetry in the rotor.

It is shown in the previous section that the unbalance orientation angle does influence the response of the two-crack rotor. Similar simulations are also repeated here in the case of an asymmetric rotor with a fatigue crack in order to understand if the results of the previous simulations in this section are valid irrespective of the unbalance orientation angle (β). Figure 12 shows the orbit plot for four different values of β for an asymmetric rotor with a fatigue crack oriented at an angle of 180°. The orbit plot slightly changes orientation of its inner loop for $\beta = 90$ and 270°, for which the inner loop gets pulled in the direction of the unbalance. The changes in the orbit plot are not very substantial and can be explained by the fact that the speed of the rotor is of a low order (1/10th of the first bending critical speed). Thus at such a low speed the effect of unbalance orientation can be expected to be marginal. However, the simulations are carried out to study the effect of a different unbalance orientation angle ($\beta = 90^\circ$) than the one previously considered ($\beta = 0^\circ$) on the orbit plot changes due to different crack orientation angle (γ). Figures 13 and 14 show the response of an asymmetric rotor without and with the crack at different orientations with the direction of asymmetry of unbalance orientation angle of $\beta = 90^\circ$.

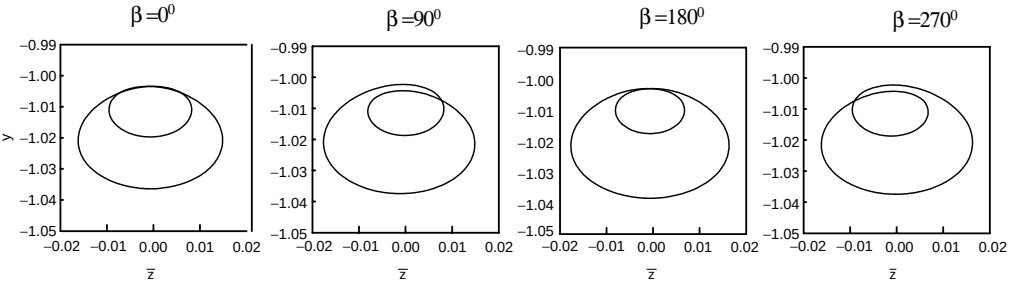

Figure 12. Effect of unbalance orientation angle (β) on the orbital response of an asymmetric rotor with crack $\bar{a}_1 = 0{\cdot}2$, $\bar{a}_2 = 0{\cdot}2$, $\gamma = 180^\circ$ and $r_{unb} = 0{\cdot}1$.

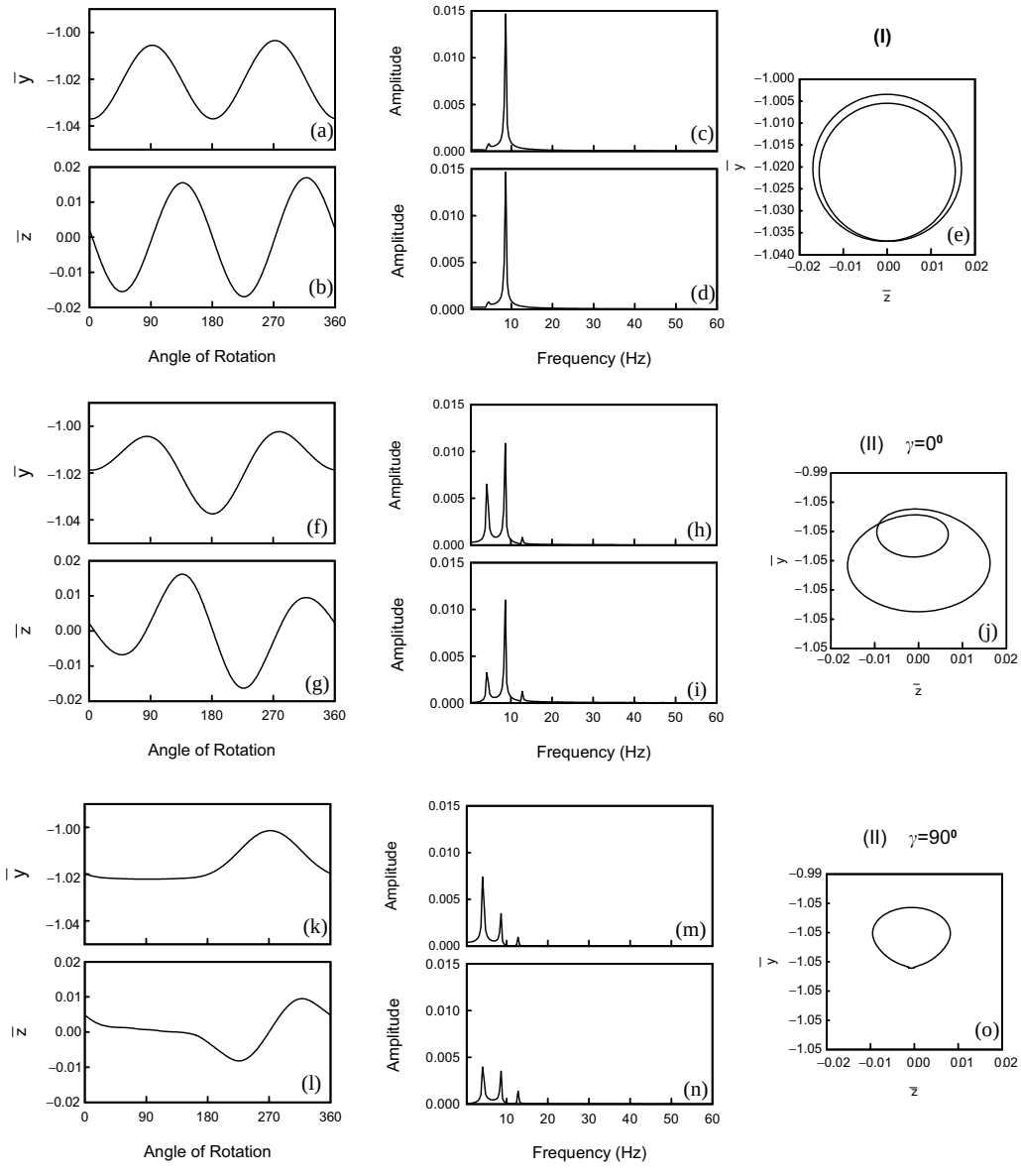

Figure 13. Response of an asymmetric rotor with $\bar{a}_1 = 0{\cdot}2$, $\bar{a}_2 = 0{\cdot}2$, $r_{unb} = 0{\cdot}1$, $\beta = 90^\circ$. (I) Asymmetric rotor without crack; (II) $\gamma = 0^\circ$. (III) $\gamma = 90^\circ$. (a) Time domain response in vertical direction. (b) Time domain response in horizontal directions. (c) Frequency domain response in vertical direction. (d) Frequency domain response in horizontal direction. (e) Orbit plot.

Comparing these results with those presented in Figures 10 and 11 for $\beta = 0^\circ$, it is quite clear that the unbalance orientation angle only slightly alters the response. The frequency composition and the amplitudes of these frequencies in both the cases of β are also comparable. It can thus be concluded that the phase of unbalance relative to the crack only slightly modifies the response variation with γ. The presence of crack in an asymmetric rotor can still be identified from the changes in the orbit plot irrespective of the phase of the unbalance. The unbalance phase does not play a very dominant role at such a slow speed.

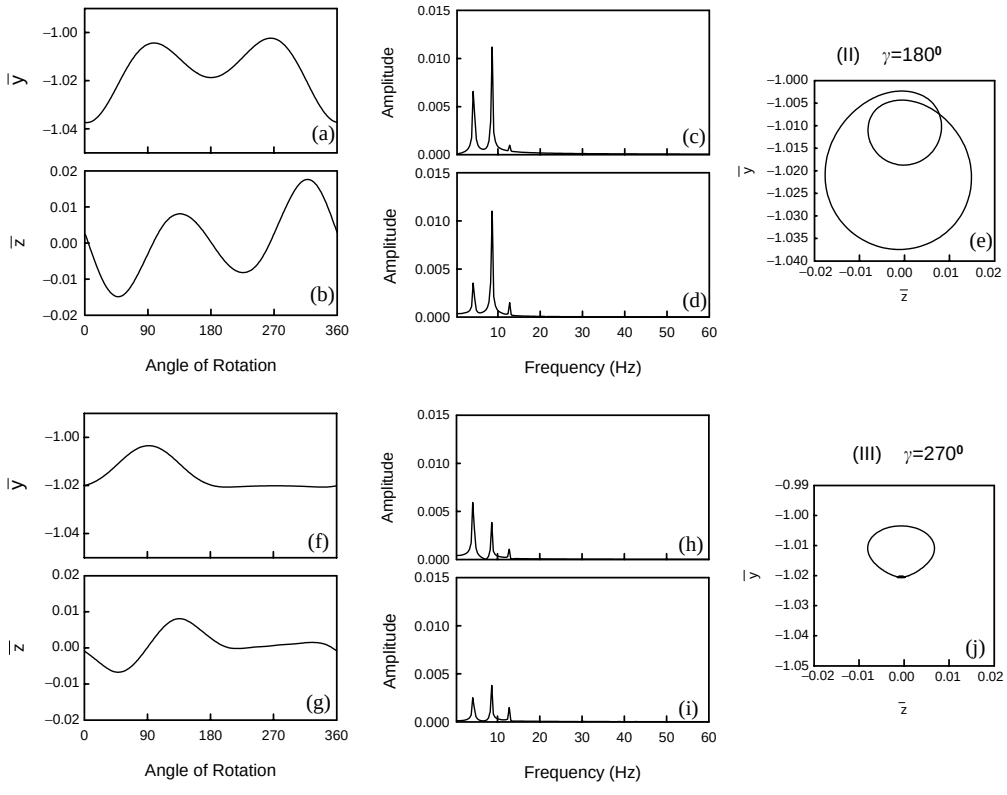

Figure 14. Response of an asymmetric rotor with a crack with $\bar{a}_1 = 0{\cdot}2$, $\bar{a}_2 = 0{\cdot}2$, $r_{unb} = 0{\cdot}1$, $\beta = 90^\circ$. (I) $\gamma = 180^\circ$. (II) $\gamma = 270^\circ$. (a) Time domain response in vertical direction. (b) Time domain response in horizontal directions. (c) Frequency domain response in vertical direction. (d) Frequency domain response in horizontal direction. (e) Orbit plot.

5. CONCLUSIONS

The stiffness of a two-crack Jeffcott rotor is derived from the concepts of fracture mechanics. The cracks are assumed to breathe as the rotor rotates. Breathing behaviour of both the cracks could be studied in detail due to the complex non-linear model used in the study. When the orientation of one crack relative to the other is varied, the breathing behaviour of the cracks changes leading to the changes in the stiffness variation that ultimately affects the response pattern of the cracked rotor. The effect of the orientation of the crack on the response is more strongly observed at lower speeds. At very high speeds close to the critical speed, this effect is not observed. The change in response could be observed in frequency domain and orbit plots. The salient features of the response of the two-crack rotor are as follows:

1. If the two cracks are aligned, the frequency response contains first three harmonics of rotational speed. If one of the cracks is oriented perpendicular to the first one, the second harmonic component vanishes from the spectrum. When the two cracks are in opposite phase, the third harmonic component is absent and the second harmonic component of vibration becomes very dominant.
2. The orbit plot shows significant changes. From the onion shape for $\gamma = 0^\circ$, the orbit changes to an oblong shape for $\gamma = 90^\circ$ and then to a double looped orbit for $\gamma = 180^\circ$.

3. For higher speeds near half the uncracked shaft critical speed, the changes are seen more prominently at $\gamma = 90^\circ$, where the second harmonic component of the spectrum almost vanishes, and the orbit plot does not show the characteristic inner loop which is other wise shown at this period.
4. The unbalance orientation angle (β) has shown its influence on the orbit plot in the case of a two-crack rotor. The nature of this influence is dependent on crack orientation angle (γ). When β is varied, the orientation of the orbit alters without significant change in its shape if $\gamma = 90$ or 180°, whereas the orbit shape alters slightly if $\gamma = 90^\circ$. However the influence of β is particularly noticeable at higher speeds ($r_{unb} = 0{\cdot}5$).

The presence of a breathing crack in an asymmetric rotor brings about some distinctive changes in the frequency spectrum and orbit plots of the response. The salient features of the response of an asymmetric rotor with a breathing crack are as follows:

1. The presence of a breathing crack in an asymmetric rotor adds higher harmonics in the spectrum in addition to a dominant first harmonic component. Without any crack, an asymmetric rotor exhibits very large second harmonic component and a negligible first harmonic at lower speeds.
2. The orbit plot changes could be either change in the orientation of the inner loop, its relative size or the complete disappearance of this inner loop depending upon the orientation of this crack with respect to the direction of the original asymmetry.
3. The effect of the phase of unbalance with respect to the direction of asymmetry is shown to be marginal, particularly at slower operating speeds ($r_{unb} = 0{\cdot}1$). Even for a different unbalance phase ($\beta = 90^\circ$), the orbit plot changes were found to be similar to those obtained for $\beta = 0^\circ$.

These changes could be useful in diagnosing fatigue crack in asymmetric rotors. This vibration-based diagnostic strategy has an advantage that it can be applied without bringing the rotor to a halt and taking the rotor out of service.

REFERENCES

1. J. Wauer 1990 *Applied Mechanics Reviews* **43**, 13–17. Dynamics of cracked rotors: literature survey.
2. A. D. Dimarogonas 1996 *Engineering Fracture Mechanics* **55**, 831–357. Vibration of cracked structures: a state of the art review.
3. W. M. Ostachowicz and M. Krawczuk 1991 *Journal of Sound and Vibration* **150**, 191–201. Analysis of effect of cracks on the mutual frequencies of a cantilever beam.
4. M.-H. H. Shen and C. Pierre 1990 *Journal of Sound and Vibration* **138**, 115–134. Natural modes of Bernoulli–Euler beams with symmetric cracks.
5. R. Ruotolo, C. Surace and C. Mares 1996 *Proceedings of the* 14*th International Modal Analysis Conference*, 1560–1564. Theoretical and experimental study of the dynamic behaviour of a double-cracked beam.
6. R. Ruotolog and C. Surace 1997 *Journal of Sound and Vibration* **206**, 567–588. Damage assessment of multiple cracked beams: numerical results and experimental validation.
7. M. H. Shen and J. E. Taylor 1991 *Journal of Sound and Vibration* **206**, 457–484. An identification problem for vibrating cracked beams.
8. R. Ruotolog and C. Surace 1996 *Proceedings ISMA21, Leuven, Belgium*, 1005–1016. Damage assessment for a beam with multiple cracks.
9. A. S. Sekhar 1999 *Journal of Sound and Vibration* **223**, 497–512. Vibration characteristics of a cracked rotor with two open cracks.
10. A. W. Lees and M. I. Friswell 2000 *Proceedings of the Conference on Advances in Structural Dynamics, ISVR, Southampton, June* 2000. The vibration signature of chordal cracks in asymmetric rotors.

11. O. S. Jun, H. J. Eun, Y. Y. Earmme and C. W. Lee 1992 *Journal of Sound and vibration* **155**, 273–290. Modeling and vibration analysis of a simple rotor with a breathing crack.
12. H. Tada, P. C. Paris and G. R. Irwin 1973 *The Stress Analysis or Crack Handbook*. Hellertown, PA: Del Research Corporation.
13. A. Tondl 1965 *Some Problems of Rotor Dynamics*. London: Chapman & Hall.
14. B. Grabowski 1984 *Dynamics of Rotors—Stability and System Identification CISM Courses and Lectures*, Vol. 273. New York: Springer. The vibrational behaviour of a rotting shaft containing a transverse crack.
15. I. W. Mayes and W. G. R. Davies 1984 *Journal of Vibration, Acoustics, Stress, and Reliability in Design* **106**, 139–145. Analysis of the response of a multi-rotor-bearing system containing a transverse crack in a rotor.

APPENDIX A: NOMENCLATURE

$\xi_1-\eta_1$	co-ordinate system for crack 1
$\xi_2-\eta_2$	co-ordinate system for crack 2
γ	angle made by crack 2 relative to crack 1
a_1, a_2	depth of cracks 1 and 2 respectively
D	diameter of the shaft
$\bar{a}_1, \bar{a}_2$	crack depth ratio (a/D) for cracks 1 and 2 respectively
L	length of the shaft
m	mass of the disc
c	damping constant
ζ	damping factor
ε	eccentricity of mass of disc from its geometric center
δ_{st}	static deflection of the uncracked rotor
e	dimensionless eccentricity (e/δ_{st})
β	orientation of centre of mass from ξ_1 axis in the direction of shaft rotation
θ	angle of rotation of shaft
y, z	rotor center displacement in vertical and horizontal direction respectively
ξ_1, η_1	rotor center displacement in the direction perpendicular to crack edge and in the direction parallel to crack edge of crack 1 respectively
ξ_2, η_2	rotor center displacement in the direction perpendicular to crack edge and in the direction parallel to crack edge of crack 2 respectively
k_0	uncracked rotor stiffness
k_ξ, k_η	direct stiffness of the shaft in ξ_1 and η_1 direction respectively
$k_{\xi\eta}, k_{\eta\xi}$	cross-coupled stiffnesses
ω	rotational speed in rad/s
t	time in seconds
g_ξ, g_η	flexibility in ξ_1 and η_1 directions respectively
$g_{\xi\eta}, g_{\eta\xi}$	cross-coupled flexibilities
Q_{ξ_1}, Q_{η_1}	forces acting on the shaft at cross-section of crack 1 in ξ_1 and η_1 directions respectively
Q_{ξ_2}, Q_{η_2}	forces acting on the shaft at cross-section of crack 1 in ξ_2 and η_2 directions respectively
K_1^I, K_2^I	total stress intensity factor at any point along the crack edge of cracks 1 and 2 respectively
$K^I_{Q_{\xi_1}}, K^I_{Q_{\eta_1}}$	stress intensity factor due to forces Q_{ξ_1} and Q_{η_1} respectively